ELSEVIER

Chemical Geology 235 (2006) 325–351

CHEMICAL GEOLOGY
INCLUDING
ISOTOPE GEOSCIENCE

www.elsevier.com/locate/chemgeo

Noble gas and halogen constraints on mineralizing fluids of metamorphic versus surficial origin: Mt Isa, Australia

M.A. Kendrick [a,*], R. Duncan [b], D. Phillips [a]

[a] *Predictive Mineral Discovery Cooperative Research Centre (pmd*CRC), The School of Earth Sciences, University of Melbourne, Victoria 3010, Australia*

[b] *Predictive Mineral Discovery Cooperative Research Centre (pmd*CRC), The School of Geosciences, Monash University, Victoria, 3800 Australia*

Received 8 March 2006; received in revised form 14 July 2006; accepted 5 August 2006

Editor: D. Rickard

Abstract

The origin of hydrothermal fluids responsible for silica–dolomite alteration associated with Cu ore in the giant Mt Isa deposit of Queensland, north east Australia has been investigated. Main-stage quartz and dolomite veins, and late- to post-ore quartz from the Buck Quartz Fault in the orebody footwall, plus the regional Mt Isa and Railway Faults contain two phase liquid–vapour fluid inclusions with variable salinity.

Fluid inclusion molar Br/Cl values are mostly in the range $1.5–12\times10^{-3}$ and molar I/Cl values are in the range $9–186\times10^{-6}$. Greater than seawater Br/Cl and I/Cl values can characterise either sedimentary formation waters with a bittern brine origin by the sub-aerial evaporation of surface water beyond the point of halite saturation or some metamorphic dehydration fluids with a deep crustal source. We propose that these alternative origins can be distinguished in our samples based on the relationship between $^{40}Ar/^{36}Ar$ and ^{36}Ar concentration.

Metamorphic fluids formed by dehydration of crystalline rock are predicted to have low ^{36}Ar concentrations with the salinity, $^{40}Ar/^{36}Ar$ and $^{40}Ar_E/Cl$ values determined by the whole rock concentration of Cl, ^{36}Ar, OH^-, K and age. The main-stage quartz and Buck Quartz Fault samples host fluid inclusions with <20 wt.% NaCl eq., 1–3 ppb ^{36}Ar, $^{40}Ar/^{36}Ar$ in the range ~10,000–28,000 and high $^{40}Ar_E/Cl$ values of $\sim3–8\times10^{-4}$. These values are consistent with metamorphic fluids sourced by devolatilisation of either the underlying Eastern Creek Volcanics or the Barramundi Basement.

In contrast, surface-derived fluids acquire elevated $^{40}Ar/^{36}Ar$ values (>296) through fluid–rock interaction which leads to a simultaneous increase in ^{36}Ar concentration. The main-stage Ca-rich dolomite fluid inclusions have high salinities close to the point of halite saturation (~26 wt.%), 1.7–5.5 ppb ^{36}Ar, $^{40}Ar/^{36}Ar$ in the range 1600–8400 and $^{40}Ar_E/Cl$ of $\sim0.2–1\times10^{-4}$. These values are most similar to those expected in an evolved bittern brine; however, the ^{36}Ar concentration and $^{40}Ar/^{36}Ar$ value exhibit a weakly negative correlation, which is the opposite to that expected in surface-derived fluids.

Only fluid inclusions in samples from the Railway Fault and some fluid inclusions in samples from the Buck Quartz Fault have ^{36}Ar concentrations of greater than Air Saturated Water (ASW = 1.3–2.7 ppb ^{36}Ar), up to 27 ppb, and $^{40}Ar/^{36}Ar$ values of ~1000–2500 that are expected for fluids with an exclusively sedimentary formation water origin. Fluid inclusions in the Mt Isa Fault samples have the highest ^{36}Ar concentrations of up to ~100 ppb, some of the lowest $^{40}Ar/^{36}Ar$ values and the highest Br/Cl value of up to $\sim30\times10^{-3}$. These features distinguish it from all other sample groups in the mine area.

Silica–dolomite alteration (and Cu mineralization) are interpreted to have resulted from mixing of the deeply derived metamorphic fluid, best preserved in quartz fluid inclusions, and a surface-derived bittern brine, partially preserved within the

* Corresponding author.
E-mail address: mark.kendrick@unimelb.edu.au (M.A. Kendrick).

0009-2541/$ - see front matter
doi:10.1016/j.chemgeo.2006.08.002

main-stage dolomite fluid inclusions. Inflow of a second surficial fluid, along regional faults and into the mine through the late- to post-D_3 Buck Quartz Fault may have terminated mineralization. The involvement of metamorphic fluids is compatible with the syn-D_3 (~1530 Ma) timing of mineralization during the final stages of the Isan orogeny.

Keywords: Argon isotopes; Br/Cl-I/Cl; Deep-crustal fluids; Proterozoic; Giant Cu-ore deposit

1. Introduction

The Proterozoic Mt Isa Inlier of northeast Australia is richly endowed with several distinct styles of ore deposit, but the spatial association of giant breccia-hosted Cu orebodies (255 Mt at 3.3% Cu) with giant stratiform Pb–Zn orebodies (150 Mt at 6% Pb and 7% Zn) within a single mine at Mt Isa is unique (Fig. 1; McGoldrick and Large, 1998; Waring et al., 1998). The origin and relative timing of the orebodies remains controversial with various syn-sedimentary/diagenetic and epigenetic models proposed (e.g. McDonald, 1970; Perkins, 1984; Swager, 1985; Bell et al., 1988; McGoldrick and Keays, 1990; Hannan et al., 1993; Heinrich et al., 1995; Perkins and Bell, 1998; Carr et al., 2004; Davis, 2004). However, most workers agree that the breccia-hosted Cu-mineralisation is genetically related to extensive syn-deformational (epigenetic) silica and dolomite alteration that in itself represents a massive hydrothermal event and occurred during the ~1600–1500 Ma Isan Orogeny (Perkins, 1984; Swager, 1985; Bell et al., 1988; Heinrich et al., 1989; 1995; Perkins et al., 1999; Carr et al., 2004; Betts et al., 2006).

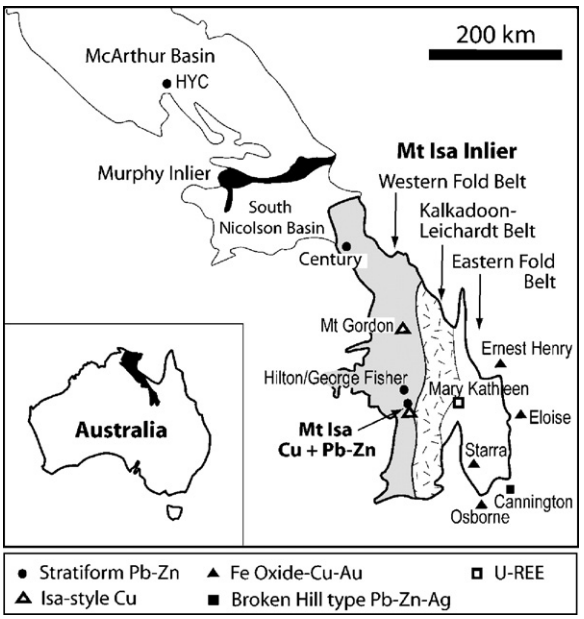

Fig. 1. Map showing the positions of selected world class ore deposits in the Mt Isa Inlier and McArthur Basin of northeast Australia.

In order to better constrain the origin of Isa-style Cu-mineralization we have investigated the noble gas and halogen geochemistry of fluid inclusions trapped within main-stage quartz and dolomite veins. The new chemical parameters are important because they constrain hydrothermal fluids that based on stable isotope data and quartz fluid inclusion Br/Cl values alone could represent either surface-derived but highly evolved sedimentary formation water that acquired salinity by sub-aerial evaporation beyond the point of halite saturation (e.g. bittern brines) or metamorphic fluids with a deep crustal source (Zherebtsova and Volkova, 1966; Heinrich et al., 1989; 1993; Svensen et al., 2001).

The $^{40}Ar/^{36}Ar$ value of a fluid can help distinguish between these alternatives because it varies by orders of magnitude between the hydrosphere (modern value = 295.5); near-surface sedimentary formation waters with values of less than ~2000 (Kelley et al., 1986; Böhlke and Irwin, 1992a; Turner and Bannon, 1992; Kendrick et al., 2002a,b); and deep crustal or mantle fluids with values of tens of thousand (Ozima and Podosek, 2002). Furthermore, ^{36}Ar and $^{40}Ar_E$[1] concentrations can be increased during various fluid–rock interactions and can provide insight into probable fluid source or aquifer lithology (Turner and Bannon, 1992; Kendrick et al., 2005). Iodine has a strong affinity for organic matter (e.g. Worden, 1996) and fluid I/Cl values can be increased through interaction with organic-rich sedimentary rocks.

Copper mineralization at Mt Isa is believed to have occurred at a depth of 6–8 km (Heinrich et al., 1989; Matthai et al., 2004) and the new data therefore provide the first detailed constraints on the Ar isotopic composition of hydrothermal fluids in the mid-crust. Previous combined noble gas and halogen studies have been largely limited to Phanerozoic ore deposits formed at depths of less than ~2 km (Böhlke and Irwin, 1992a,b; Irwin and Roedder, 1995; Kendrick et al., 2001a, 2002a, b, 2005), with exceptions being a Precambrian granite (Irwin and Reynolds, 1995) and iron-oxide-copper-gold

[1] $^{40}Ar_E$ = excess ^{40}Ar not derived from the atmosphere ($295.5 \times {}^{36}Ar$) or by in situ radiogenic decay of ^{40}K.

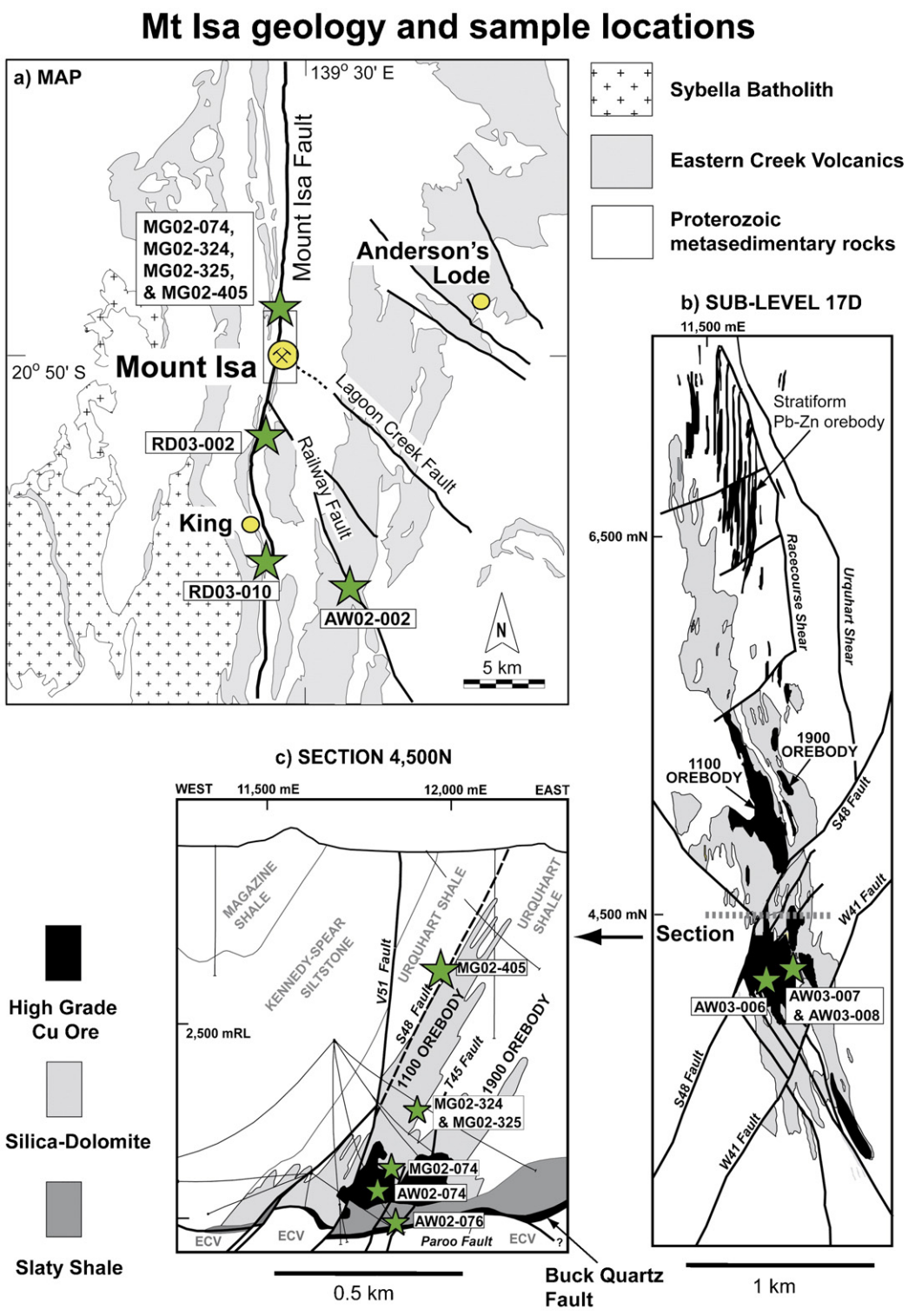

Fig. 2. (a) Geological map of the area surrounding Mt Isa (Derrick, 1976; Hill, 1978), showing the positions of Anderson's Lode U-prospect and the King locality for metasomatic tourmaline (Heinrich et al., 1995; Perkins et al., 1999; Duncan et al., in press). (b) Mine plan of sub-level 17D, and (c) mine section 4500 mN (data from unpublished Xstrata files, Mt. Isa Mine, see also Perkins (1984) and Swager (1985)).

(IOCG) deposits in Mt. Isa's Eastern Fold Belt (Kendrick et al., 2006a,b). Finally, fluid inclusions in the quartz samples are ideal for further evaluation of mechanical versus thermal decrepitation procedures (see Kendrick et al., 2006a,b) because none of the fluid inclusions examined by microscopy contain daughter minerals.

2. Geological context

2.1. Regional geology

The Mt Isa mine is situated in the Western Fold Belt of the Mt Isa Inlier, close to the N–S striking Mt Isa Fault Zone (Figs 1 and 2a). The copper orebodies and associated 'silica–dolomite' alteration are hosted by the Urquhart Shale, where it is juxtaposed against the greenschist Eastern Creek Volcanics along the Paroo Fault (Fig. 2c).

The Urquhart Shale consists of thinly bedded carbonaceous, dolomitic, pyritic shale and siltstone with tuffaceous marker beds that yield an inherited zircon U–Pb age of 1655±4 Ma (Page et al., 2000). The underlying Eastern Creek Volcanics (ECV) comprise up to 6.5 km of continental tholeiites and interlayered fluvial clastic sedimentary rocks (Bain et al., 1992) and their age of ~1780 Ma is constrained by U–Pb whole rock and detrital zircon ages (Farquharson and Richards, 1974; Neumann et al., in press). Seismic data indicate that the ~1870 Ma felsic-rich crystalline Barramundi Basement has a depth of 4.5–8.5 km in the mine area (Page and Williams, 1988; O'Dea et al., 1997; MacCready et al., 1998). The Sybella Batholith intruded to the west of the mine area at ~1670–1650 Ma (Fig. 2; Page and Bell, 1986; Connors and Page, 1995) and the regional sedimentary rocks and sequence-stratigraphy have been described in detail (Jackson et al., 2000; Page et al., 2000; Southgate et al., 2000).

Three regional deformation events were originally recognised in the Western Fold Belt (Bell, 1983; Page and Bell, 1986; see Table 1). D_1 is characterised by N–S directed thrusting (Bell, 1983) and the Paroo 'thrust' Fault juxtaposed the Urquhart Shale host rock with the ECV at this time (Fig. 2; Bell et al., 1988). D_2 developed N–S striking folds and a pervasive deformation fabric during peak metamorphism (Bell, 1983; Rubenach, 1992). The most recent opinion is that this occurred at 1585–1565 Ma synchronous with peak metamorphism in the Eastern Fold Belt (Connors and Page, 1995; Hand and Rubatto, 2002; Betts et al., 2006; Duncan et al., 2006) and was overprinted by a younger metamorphic event in the vicinity of the Sybella Batholith at 1532±7 Ma (Connors and Page, 1995; Betts et al., 2006; Duncan et al., 2006). D_3 formed NNW–SSE striking folds in 10–20 m wide shear zones that are locally 100's of metres wide and include the 200–400 m Mt Isa Fold (Bell et al.,

Table 1
Summary of constraints on the timing of regional deformation and mineralisation

Deformation event	Age constraints	Alteration/mineralisation stage
D_1: Regional N–S shortening (Bell, 1983)	1610±13 Ma Rb–Sr whole rock Sybella granite (Bell, 1983; Page and Bell, 1986)	
D_2: Regional E–W compression (Bell, 1983), peak metamorphism (Rubenach, 1992), affected entire Inlier (Betts et al., 2006)	1573±12 Ma, Pb–Pb tourmaline (Duncan et al., in press). 1540–1575 Ma U–Pb SHRIMP metm. monazites (Hand and Rubatto, 2002); preferred timing 1585–1565 Ma (Betts et al., 2006)	
Post-D_2 metamorphism in Sybella area, relationship to D_3 uncertain.	1544±12 Ma, Rb–Sr whole rock (Bell, 1983; Page and Bell, 1986). 1532±7 Ma U–Pb SHRIMP zircon (Connors and Page, 1995). 1528±51 Ma, Pb–Pb tourmaline (Duncan et al., in press)	Post-D_2 to pre-D_3, early silicification, quartz veining and dolomite recrystalisation (Perkins, 1984; Swager, 1985; Bell et al., 1988)
D_3: 'Regional' E–W compression with dextral strike slip component partitioned along corridors (ie. Mt. Isa 'Shear' Zone), N–NW striking folds and deformation fabric (Bell, 1983; Bell et al., 1988)	1523–1505 Ma, Ar–Ar biotite (Perkins et al., 1999). 1510±13 Ma, Rb–Sr whole rock (Bell, 1983; Page and Bell, 1986)	Early D_3 dolomite veining (Perkins, 1984; Swager, 1985; Bell et al., 1988), Early to late D_3 chalcopyrite brecciation±quartz±Fe-sulphide (Perkins, 1984; Swager, 1985)
Post deformational pegmatite (Sybella)	1480±14 Ma U–Pb SHRIMP pegmatitic zircon Sybella Granite (Connors and Page, 1995)	
Late-orogenic wrenching, Continued dexteral wrenching on strike-slip faults i.e. Mt Isa Fault Zone (Lister et al., 1986; O'Dea et al., 1997; Lister et al., 1999)	Post-D_3 Ar–Ar hornblende and muscovite ages from west of the Mt Isa Fault indicate that uplift relative to Mt Isa continued on the Mt Isa Fault until at least 1400 Ma (Perkins et al., 1999)	Late to post-D_3 quartz veins including the Buck Quartz (Perkins, 1984; Bell et al., 1988)

1988). D_3 is bracketed by peak metamorphism and a post-deformational pegmatite U–Pb zircon age of 1480±14 Ma (Connors and Page, 1995).

The D_3 shear zones are overprinted by N–S striking dextral brittle-faults and late-orogenic wrenching continued along these structures during the waning stages of E–W shortening (Lister et al., 1986; O'Dea et al., 1997; Lister et al., 1999). The Mt Isa Fault cuts the Mt. Isa Fold, demonstrating late-orogenic timing (Bell et al., 1988) and is a master fault in this wrench system (e.g. Betts et al., 2006). The Railway Fault has an angle of ~30° to the Mt Isa Fault (Fig. 2a) and may represent a second order fault within a riedal shear wrench setting (O'Dea et al., 1997; Betts et al., 2006). Argon–argon metamorphic cooling ages for amphibolite rocks west of the Mt Isa Fault (~1457 Ma for hornblende and ~1397 Ma for muscovite) are younger than D_3 metamorphic ages in the mine area (1523–1505 Ma for biotite; Perkins et al., 1999). These ages are similar to Ar–Ar ages obtained elsewhere in the Inlier (Spikings et al., 2002) and they suggest exhumation of the western higher-grade block relative to Mt Isa continued until at least ~1400 Ma (Perkins, 1984).

2.2. Mine geology

The lobate silica–dolomite alteration halos are subparallel to bedding with the highest copper grades occurring within mono-mineralic chalcopyrite matrix-supported breccias in the central silica-rich portion (Fig. 2; Perkins, 1984; Swager, 1985). In addition to chalcopyrite, quartz and dolomite; pyrite, pyrrhotite, cobaltite, talc, chlorite and apatite are moderately common (Mathias and Clark, 1975) and were precipitated in a multi-phase paragenetic sequence that is simplified into three stages (Perkins, 1984; Swager, 1985): (1) Early (post-D_2 to pre-D_3) dolomitisation and silicification; (2) early-D_3 crystalline dolomite veins and breccias; and finally (3) chalcopyrite±Fe-sulphide ±quartz±chlorite.

The final Cu-mineralistion stage has been variably interpreted as early-D_3 based on S_3 quartz fibres that overgrow replacive chalcopyrite (Swager, 1985) and late- to post-D_3 based on chalcopyrite in D_3 cleavages and strain free quartz (Perkins, 1984, p. 630). East-dipping chalcopyrite bearing quartz veins cut D_3-folds and post-date the main-stage of mineralization (Perkins, 1984, p. 631). These late veins have similar timing to the post-D_3 Buck Quartz Fault beneath the 3500-orebody (Bell et al., 1988, p. 75) and it is possible that these late faults are correlated with late-orogenic wrenching along the Mt Isa and Railway Faults.

The late-orogenic (~D_3) timing of Cu-mineralization is compatible with the preferred ~1523 Ma Ar–Ar biotite age for mineralization (Perkins et al., 1999). However, mineralization may have occurred slightly earlier and synchronously with post-peak metamorphism of the Sybella Batholith at 1532±7 Ma (Connors and Page, 1995). Contemporaneous hydrothermal activity elsewhere in the Fold Belt was suggested previously based on a ~1534 Ma Ar–Ar biotite age for the Anderson's Lode U prospect (Perkins et al., 1999) and is also indicated by a 1528±51 Ma Pb–Pb tourmaline age for boron metasomatism at nearby King (Fig. 2a; Duncan et al., 2006).

2.3. Fluid geochemistry

Quartz and dolomite alteration veins in the mine area are dominated by two phase liquid–vapour fluid inclusions that do not preserve evidence of fluid boiling (Heinrich et al., 1989). Relative to VSMOW, quartz fluid inclusions are estimated to have $\delta^{18}O_{fluid}$ of 1–6‰ and inclusion extracts have δD_{fluid} of −35 to −72‰; dolomite fluid inclusions are estimated to have $\delta^{18}O_{fluid}$ of 4–9‰ and inclusion extracts have $\delta D_{fluid} \approx -29$‰ (Fig. 11 of Heinrich et al., 1989). Relative to PDB, the $\delta^{13}C_{fluid}$ estimated for CO_2–CH_4-bearing NaCl-rich fluid is between −6‰ and −20‰ (Heinrich et al., 1989). Relative to CDT, chalcopyrite, pyrite and pyrrhotite have $\delta^{34}S_{sulphide}$ in the range 8–21‰ that are ^{34}S-enriched relative to the Eastern Creek Volcanics (Andrew et al., 1989; Hannan et al., 1993). Molar Br/Cl values previously determined by neutron activation analysis of quartz are $3.5–8.0\times10^{-3}$, on average 3.5 times the modern day seawater value (Heinrich et al., 1993).

Together the fluid inclusion and stable isotope data indicate Cu-mineralization occurred between 350 °C and 2.5 kbars and, 200 °C and 0.6 kbars, corresponding to a near lithostatic pressure and a preferred depth of 6–8 km (Andrew et al., 1989; Heinrich et al., 1989; Matthai et al., 2004). The $\delta^{13}C_{fluid}$ is lower than expected for a magmatic fluid, and Heinrich et al. (1989) proposed an origin from either an evaporite-derived metamorphic fluid or an evolved bittern brine sedimentary formation water. The previously published greater than seawater Br/Cl values, preclude evaporite-dissolution which leads to low Br/Cl values (Holser, 1979), and are compatible with the bittern brine hypothesis (Heinrich et al., 1993). The ^{34}S-enriched ore minerals suggest S was sourced from sedimentary rocks or seawater sulphate compatible with bittern brine involvement (Andrew et al., 1989; Hannan et al., 1993).

However, it is now known that high, greater than seawater, Br/Cl values characterise some high-grade metamorphic fluids (Svensen et al., 2001) and a metamorphic fluid origin is compatible with the syn-D_3 timing of mineralization (Perkins, 1984; Swager, 1985; Bell et al., 1988), and the stable isotope and elemental geochemistry of the variably altered Eastern Creek Volcanics (Hannan et al., 1993). Therefore, the currently

Table 2
Sample descriptions

Name	Location	Description	Stage [a]
Mt. Isa Mine			
a. Dolomite alteration/veins			
MG02-325A	Drill core ISA681040 1045 mRL 341086 7709503 AMG	Early stage-II crystalline dolomite-vein with fine quartz selvedge hosted by Urquhart Shale. Galena and relatively late chalcopyrite plus pyrite are occasionally present (Fig. 3f).	Early stage-II
MG02-325B	Drill core ISA681040 1045 mRL 341086 7709503 AMG	Later stage-II fine-grained crystalline dolomite-vein with coarse grained pyrite (Fig. 3f).	Later stage-II
MG02-324	Drill core ISA 681040 999.40 mRL 341069 7709502 AMG	Crystaline dolomite-vein hosted in Urquhart Shale (Fig. 3e).	Stage II
MG02-074	Drill core ISA930811 1754.3 mRL 340813 7709408 AMG	Crystalline dolomite-vein with later chalcopyrite along grain boundaries plus minor pyrite, sphalerite and cobaltite. Hosted by recrystallised dolomitic Urquhart Shale.	Stage II
MG02-405	Drill core ISA890412 406 mRL 341307 709479 AMG	Crystalline dolomite-vein with fine grained pyrite along grain boundaries, also contains chlorite.	Stage-II
b. Silica alteration/veins			
AW02-074	Drill core Q0FDEC3 approx. 1900 mRL 3409600 7706225 AMG	Elongate quartz with undulose extinction and fibrous structure from chalcopyrite-cemented hydrothermal-breccia, includes Mg-chlorite impurities (XRD). Interpreted to be representative of early stage-III mineralization because it is overprinted by carbonate and sulphide veins (Fig. 3c).	Early stage-III
AW02-076	Drill core Q0FDEC3 approx. 1910 mRL 3409650 7706250 AMG	Deformed Urquhart Shale hosted quartz vein with pyrite-rich slaty-shale breccia fragments; Overprinted by carbonate veins cut by C-rich opaque material. XRD demonstrates the presence of muscovite and Mg-chlorite (Fig. 3d).	Stage-III
AW03-008	X41 mine, 19 level 340740 7706010 AMG	Quartz vein bearing minor chalcopyrite cutting Urquhart Shale. SEM confirms TiO_2 and zircon in quartz as well as cobaltite and phlogopite (Fig. 3b).	Stage-III or later
c. Buck Quartz fault footwall to ore bodies			
AW03-006	X41 mine, 19 level 340740 7705950 AMG	Massive white quartz with vuggy cavities containing euhedral quartz crystals <5 mm. Acicular aggregates of included phlogopite needles indicated by SEM/EDAX are common (Fig. 3a).	Late stage-III to late-orogenic
AW03-007	X41 mine, 19 level 340875 7706040 AMG	Massive milky white quartz from close to late fault contact. Traces of pale green discoloration (<1%) maybe secondary copper.	Late stage-III to late-orogenic
Outside Mine area			
d. Railway Fault—13 km SSW of the mine			
AW02-002a	Outcrop GR 344770 7694060 AMG	Massive zoned quartz vein containing abundant primary fluid inclusions with accidentally trapped mica (Kendrick et al., 2006a,b; see Fig. 3G).	Late-orogenic
AW02-002b			
AW02-002c			
AW02-002d			

Table 2 (*continued*)

Name	Location	Description	Timing[b]
Outside Mine area			
e. Mt Isa Fault Zone—4.5 to 13 km south of mine			
RD04-002	Outcrop GR 342446 7701683 AMG	Massive vuggy quartz vein with limonitic staining at the contact of Moondarra Siltstone and Breakaway Shale. Chalcopyrite and pyrite mineralization postdate quartz.	Late-orogenic
RD03-010A-I	Outcrop GR 340438 7692552 AMG	Early-stage euhedral quartz vein (barren) hosted by the Breakaway Shale (Fig. 3H).	Late-orogenic
RD03-010A-II	Outcrop GR 340438 7692552 AMG	Late-stage chalcopyrite and Au bearing quartz vein hosted by the Breakaway Shale. Barite is also present in minor amounts (Fig. 3H).	Late-orogenic

[a] Paragenetic stages after Swager (1985), but constraints of Perkins (1984) and Bell et al. (1988) reviewed in Section 2 are considered.
[b] Timing interpreted from orientation of Faults and literature reviewed in Section 2.

available geochemical data are compatible with either a metamorphic fluid or an evolved bittern brine.

3. Samples and microthermometry

Main-stage dolomite and quartz samples, representative of alterations stages II and III (Swager, 1985), have been selected from sulphide-bearing and barren dolomite- and quartz-veins within the 3500 and 1100 orebodies (Table 2; Figs. 2 and 3). Additional samples have been selected from the 10 m thick Buck Quartz Fault beneath the 3500 orebody, and from the Mt Isa and Railway faults outside of the mine area (Fig. 2). This was undertaken to test if similar hydrothermal fluids passed through main-stage quartz and dolomite veins in the alteration halo, and late-orogenic quartz veins in regional faults. Fluid inclusion microthermometry indicates that all of the fluid inclusions are two phase liquid–vapour and that only three of the four previously described fluid inclusion groups are present in our samples (Fig. 4; Heinrich et al., 1989):

Dolomite vein samples (alteration-stage II) are dominated by primary, two phase liquid–vapour fluid inclusions (group 1) with final ice melting temperatures of −20 to −30 °C. Heinrich et al. (1989) reported a Na/Ca value of ~3:1 for these inclusions, but as daughter minerals are absent, the lowest ice melting temperatures together with the ternary H_2O–$CaCl_2$–NaCl phase diagram (Yanatieva, 1946) imply further Ca enrichment in some fluid inclusions. Consequently, salinities close to halite saturation are estimated as ~20–26 wt.% NaCl–$CaCl_2$ eq. Group 2, two phase liquid–vapour fluid inclusions with lower final ice melting temperatures of zero to −4 °C (Fig. 4) indicating salinity of less than ~6.5 wt.% NaCl eq. are present in samples MG02-074 and MG02-325a,b only. Both groups of dolomite fluid inclusions have maximum homogenisation temperatures of 250 °C (Fig. 4). Quartz vein samples (alteration stage III) are dominated by primary, two phase liquid–vapour fluid inclusions (group 3) with final ice melting temperatures of −5 to −17 °C, that correspond to salinities of 8–20 wt.% NaCl eq., and homogenisation temperatures of 140–220 °C (Fig. 4; Heinrich et al., 1989).

The Buck Quartz Fault samples contain primary, two phase liquid–vapour fluid inclusions, a significant number of which overlap group 3 with respect to both homogenisation temperature and salinity. However, lower salinity (8 to <1 wt.% NaCl eq.) fluid inclusions are also present (Fig. 4). The Mt Isa Fault samples contain two phase liquid–vapour fluid inclusions with homogenisation temperatures similar to group 3, but only sample RD03-002 contains fluid inclusions with similar salinities (up to ~17 wt.% NaCl eq.) and samples RD02-010A-I and -II are dominated by low salinity (<6 wt.% NaCl eq.) fluid inclusions. Primary, two phase liquid–vapour fluid inclusions define visible zoning within the Railway Fault Sample AW02-002 (Fig. 3G), they have variable salinity with the majority between 5 and 19 wt.% NaCl eq. and extremely variable homogenisation temperature (Fig. 4; Kendrick et al., 2006a).

4. Noble gas and halogen methodology

This study builds on the work of Kendrick et al. (2006a) and further evaluates the efficiency of thermal (stepped heating of uncrushed samples) versus mechanical decrepitation (in vacuo crushing) using quartz samples with fluid inclusions that do not include daughter minerals. Dolomite was analysed by *in vacuo* crushing only because it is unstable above ~800 °C making it unsuitable for stepped heating analysis in our current apparatus.

High purity mineral separates (1–3 mm) obtained by hand picking under a binocular microscope were cleaned in an ultrasonic bath using distilled water and acetone, packed into individual Al-foil capsules, placed inside a silica glass tube together with Ar–Ar irradiation monitors (Hb3Gr, GA1550) and irradiated for 150 MW h in

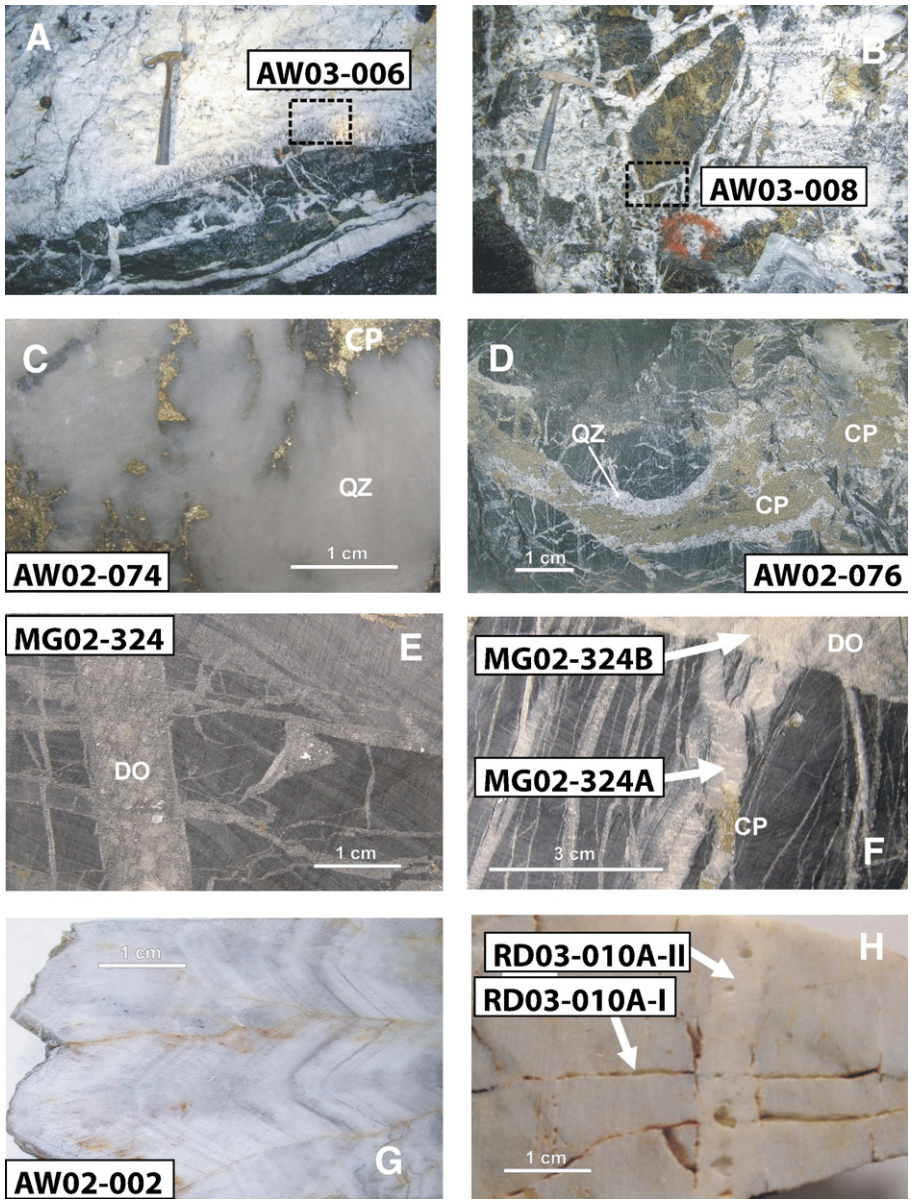

Fig. 3. Typical samples selected for analysis. (A–B) The underground localities of the Buck Quartz Fault vein samples. (C–D) Typical copper-mineralised quartz veins, hosted by Urquhart Shale, in the 1100 orebody (CP = chalcopyrite; QZ = quartz). (E–F) Dolomite veins hosted by Urquhart Shale with minor amounts of chalcopyrite (CP). (G) Euhedral quartz from the Railway Fault, detectable Cu (PIXE analysis) is assumed to be in fluid inclusions. (H) Quartz veins from the Mt. Isa Fault Zone.

position 5c of the McMaster Nuclear Reactor, Canada (Irradiation designated UM#7 on the 7th of July 2004). Mean irradiation parameters were calculated as $J = 0.0175 \pm 0.0003$; $\alpha = 0.62 \pm 0.06$ and $\beta = 5.2 \pm 0.2$; indicating a combined fast and thermal neutron fluence of $\sim 10^{19}$ n cm^{-2} (Kelley et al., 1986; Kendrick et al., 2006a).

Stepped heating of 70–120 mg samples, in an Ultra High Vacuum (UHV) tantalum resistance furnace, was achieved cyclically from an idle temperature of 100 °C up to the specified temperature over a period of 3 min. The steps had a 20 min duration and increased from 200 °C up to 700 °C in increments of 50–100 °C, but from 700 °C up to 1560 °C in increments as large as 200–400 °C. Sequential *in vacuo* crushing was achieved in modified nupro valves on 30–50 mg samples in 4–9 extraction steps.

In both cases the extracted gases were expanded through an UHV extraction line and purified on SAES

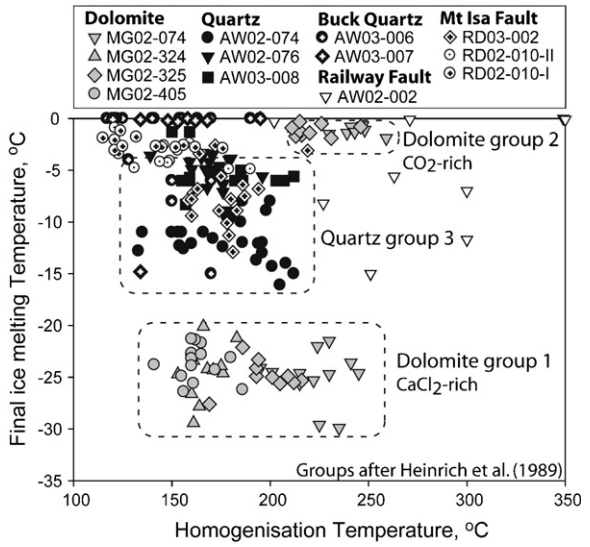

Fig. 4. Microthermometric data for the two phase liquid vapour fluid inclusions in quartz and dolomite vein samples. Samples MG02-325A and B are not distinguished in this figure.

getters over a period of 20 min before admission to the MAP-215 (Mass Analyser Products) noble gas mass spectrometer at the University of Melbourne. The purified Ar, Kr and Xe isotopes were simultaneously analysed over a period of 50 min in 9 cycles of measurement. Argon was measured on the Faraday detector while the less abundant Kr and Xe isotopes were measured at a relative gain of ~400 on a Johnson electron multiplier.

Isotopes with a measurable machine blank, expressed as a proportion of the gas released from samples, had typical values in the 200–700 °C range, of: $^{128}Xe_I$<0.1%; $^{80}Kr_{Br}$<1%, but occasionally 5%; ^{84}Kr~10% and ^{40}Ar~1–10% with an atmospheric $^{40}Ar/^{36}Ar$ ratio. Typical crusher blanks were ≪0.1% for ^{40}Ar and when ^{36}Ar was measured $^{40}Ar/^{36}Ar$ equaled the atmospheric value; Kr and Xe isotopes were beneath the multiplier detection limit of $1–2\times10^{-19}$ mol. The machine blank was only significant for stepped heating analysis of samples RD03-010A-I and -II, as these samples contain relatively few low salinity fluid inclusions. The gas abundances for each extraction step and the sample masses are tabulated in the appendix.

Analytical precision determined by the reproducibility of air calibrations is at the 0.1% level for Ar isotope ratios, but at a lower level of 3–5% for Kr/Ar and Xe/Ar ratios determined using both detectors. Total uncertainty in Br/Cl and I/Cl values is determined by the relative flux of thermal to resonant neutrons and is estimated at 10% for Br/Cl and 15% for I/Cl (Kendrick et al., 2006a). Resonant neutron correction factors of 1.5 for Br and 2.0 for I are based on the analysis of a known sample (Qtz 2320) and selected sample duplicates that have been included in five irradiations. The absolute uncertainty in sample K abundance (ppm) is at the ~20% level, this is because mass spectrometer sensitivity calibrations were less frequent than ratio calibrations. All ratios are molar and uncertainties are quoted at the 1σ level.

5. Fluid inclusion noble gas and halogen compositions

5.1. Halogen technique comparison

The two phase fluid inclusions in the Mt Isa quartz samples yielded similar Br/Cl values by stepped heating and by *in vacuo* crushing, and where there is a difference it is non-systematic (Fig. 5). This is compatible with previously reported differences in the Br/Cl and I/Cl values determined by these techniques being partly attributed to the presence of fluid inclusion daughter minerals that when present retain $^{38}Ar_{Cl}$ and degas preferentially during stepped heating (Kendrick et al., 2001b, 2006a).

Minor populations of fluid inclusions were revealed in sample AW02-074 by *in vacuo* crushing but not stepped heating (P2 in Fig. 5a), and in samples AW03-006 and 7 by stepped heating but not *in vacuo* crushing (P3 in Fig. 5b). Possible explanations for this are that *in vacuo* crushing could preferentially decrepitate small secondary fluid inclusions (<2 μm) that were aligned along planes of weakness, but were undetected during microthermometry. Such small fluid inclusions may remain intact during stepped heating. Alternatively, under different circumstances *in vacuo* crushing could break open unrelated types of fluid inclusions that due to their different physical characteristics are decrepitated at different temperatures during stepped heating (Kendrick et al., 2006a,b). The final possibility is that the data are explained by real differences between the sample splits analysed.

Exceptionally high Br/Cl values were obtained from fluid inclusions in sample RD03-010A-II by *in vacuo* crushing and the stepped heating data for this sample and sample RD03-010A-I are scattered (Fig. 5d). Although the variation could be accounted for by any of the previous explanations, in this case the *in vacuo* crushing data is preferred, because the low gas abundances released by stepped heating were affected by a significant machine blank (Section 4).

5.2. Br/Cl and I/Cl variation

Excluding the minor fluid inclusion populations identified as P2 and P3 on Fig. 5, the Br/Cl and I/Cl

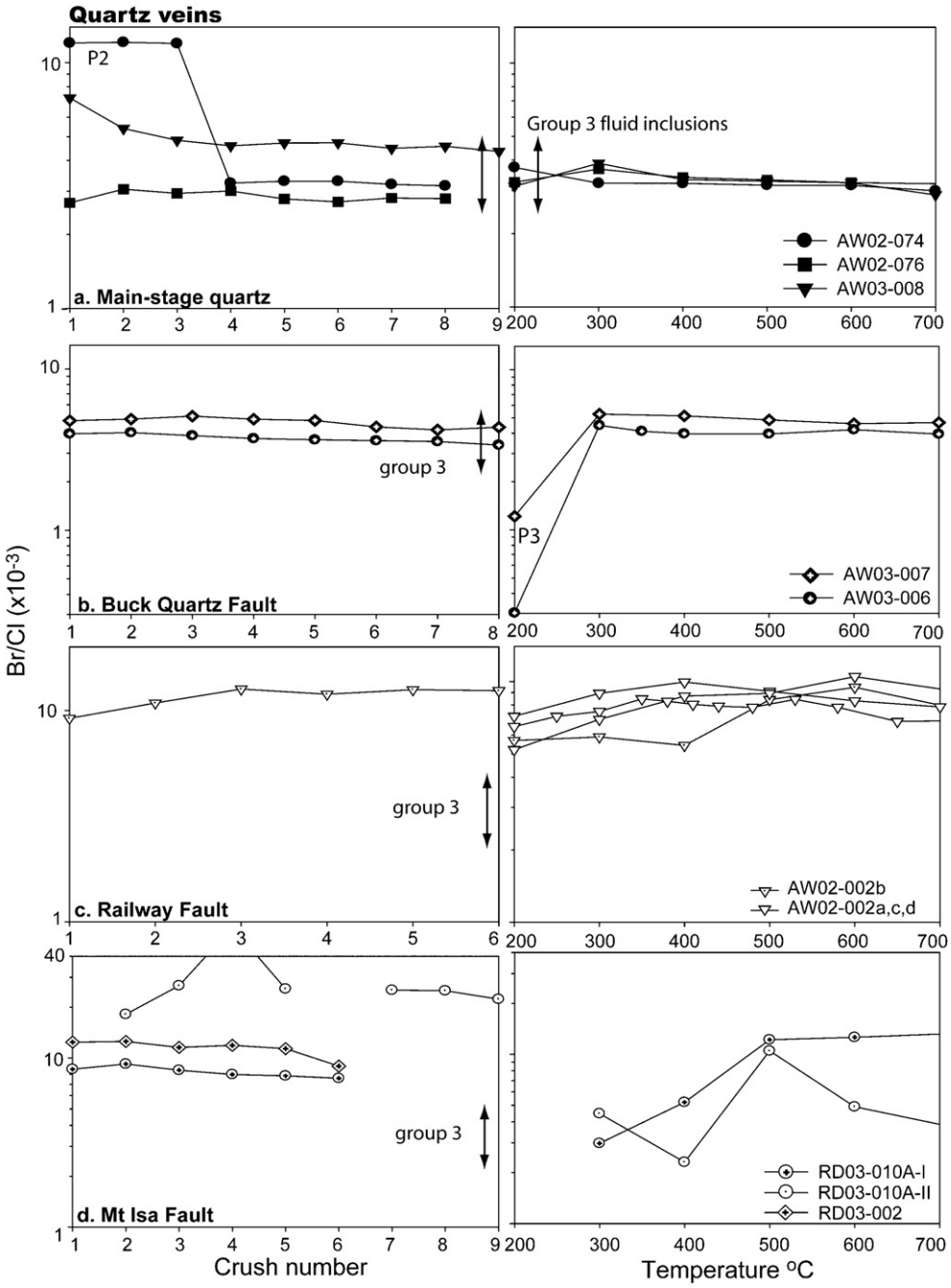

Fig. 5. Intra-sample molar Br/Cl variation for quartz samples as a function of sequential crush number and stepped heating extraction temperature; (a) main-stage quartz, (b) Buck Quartz, (c) Railway Fault, (d) Mt Isa Fault samples.

values obtained for fluid inclusions in main-stage dolomite and quartz samples vary by less than 5% or 10% (Fig. 6, Table 3). The fluid inclusions in the quartz samples exhibit slightly greater variation than fluid inclusions in the dolomite samples, but this is probably because the dolomite samples were analysed by *in vacuo* crushing only. The uniform signatures are consistent with the predominance of a single fluid inclusion 'group' within each of the main-stage quartz and dolomite samples (Section 3, Fig. 4).

Group 1 dolomite fluid inclusions with ~20–26 wt.% NaCl–$CaCl_2$ eq. have the lowest mean Br/Cl values of $1.5–4.3\times10^{-3}$ and the highest mean I/Cl values of $24–186\times10^{-6}$ (Fig. 6). The low abundance and low

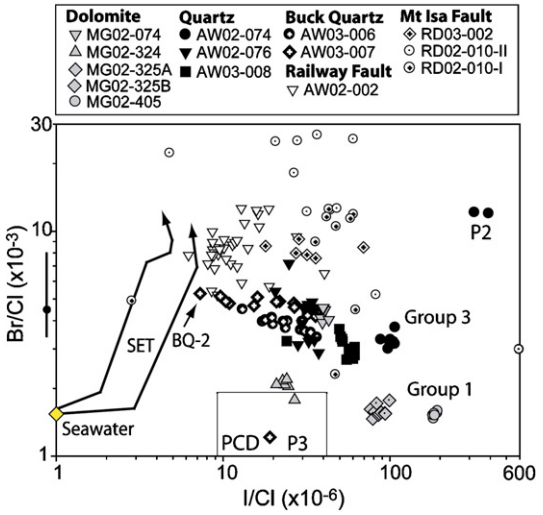

Fig. 6. Log–log molar Br/Cl versus I/Cl plot for Mt. Isa dolomite and quartz samples, in vacuo crushing and stepped heating (200–700 °C) data. The range and mean of molar Br/Cl values previously reported for Mt Isa quartz samples (Heinrich et al., 1993) are shown as a vertical bar by the *y*-axis. The seawater evaporation trajectories (SET, Zherebtsova and Volkova, 1966) and the composition of porphyry copper related mineralizing fluids with a juvenile magmatic source (PCD, Kendrick et al., 2001a,b) are shown for reference. Evaporite dissolution waters are not shown because they plot of the scale with Br/Cl of $\sim 0.1 \times 10^{-3}$ (Table 4; Holser, 1979; Böhlke and Irwin, 1992a). Data from the Buck Quartz Fault samples have intra-sample I/Cl variation of 50%: One fluid inclusion group has I/Cl and Br/Cl similar to group 3. The second fluid inclusion group (BQ-2) yields compositional values nearer to the Railway Fault sample fluid inclusions. P2 and P3 refer to minor populations of secondary fluid inclusions identified in Fig. 5.

salinity of group 2 fluid inclusions (<6.5 wt.% NaCl eq.) means they are unlikely to significantly influence the Br/Cl and I/Cl values measured in the three dolomite samples that contained both groups of fluid inclusion. Compared to the dolomite, group 3 quartz fluid inclusions with 8–20 wt.% NaCl eq. have overlapping but slightly higher mean Br/Cl values of $2.9–4.7 \times 10^{-3}$ and slightly lower mean I/Cl values of $33–105 \times 10^{-6}$ (Fig. 6, Table 3).

Fluid inclusions in the Buck Quartz Fault samples exhibit intra-sample I/Cl variation of ~50% and in these samples I is negatively correlated with Br (Fig. 6). Two groups of fluid inclusion are trapped within the samples from the Buck Quartz Fault: Fluid inclusions with Br/Cl and I/Cl similar to group 3 and a second group with I/Cl extending as low as 7×10^{-6}. This second fluid inclusion group has the highest Br/Cl values that are similar to fluid inclusions in sample AW02-002 from the Railway Fault (BQ-2, Fig. 6).

Relative to the mine samples, fluid inclusions in the Railway and Mt Isa Fault samples exhibit the greatest scatter in both Br/Cl and I/Cl (Fig. 6). The mean Br/Cl values of $7.7–9 \times 10^{-3}$ for fluid inclusions in samples from the Railway Fault and $7–29 \times 10^{-3}$ for fluid inclusions in samples from the Mt Isa Fault, are the highest measured (Table 3). The lowest I/Cl values determined for fluid inclusions in samples from the Railway Fault are very close to the seawater evaporation trajectory (SET in Fig. 6; Zherebtsova and Volkova, 1966).

5.3. Sample purity and K/Cl variation

Fluid inclusion K/Cl values are obtained by *in vacuo* crushing and in low temperature stepped heating extraction steps (Kendrick et al., 2006a). The mean K/Cl values for fluid inclusions in main-stage dolomite samples are 0.05–0.09, which are lower than the mean K/Cl values of fluid inclusions in either the main-stage quartz samples (0.09–0.18) or the Buck Quartz Fault samples (0.07–0.11; Fig. 7; Table 3).

In contrast, K/Cl values determined by stepped heating at higher temperatures (>600 °C) releases $^{39}Ar_K$ from both fluid inclusions and K-mineral impurities that may be present in either the mineral matrix or accidentally trapped within the fluid inclusions (Kendrick et al., 2006b). Several of the mine samples have maximum K/Cl values of slightly greater than one, indicating the presence of minor K-mineral impurities (Table 3). However, only samples AW02-002 and RD03-010A-II have maximum K/Cl values and ppm K concentrations that are in the hundreds (Table 3).

5.4. Argon

Fluid inclusions have three sources of ^{40}Ar: Radiogenic $^{40}Ar_R$ produced *in situ* by radioactive decay of ^{40}K since the time of trapping; atmospheric $^{40}Ar_A$ ($295.5 \times {}^{36}Ar$); and excess $^{40}Ar_E$ with an independent origin. The fluid inclusions initial ^{40}Ar composition has been determined by making a correction for radiogenic $^{40}Ar_R$ based on the sample K content and a mineralization age of 1523 Ma (Perkins et al., 1999).The age correction is 0.1–2% for the majority of samples in this study, including all of the mine area samples that have less than ~50 ppm K (Table 3). Furthermore, the age-corrected $^{40}Ar/^{36}Ar$ value is within error of the measured $^{40}Ar/^{36}Ar$ value in the majority of extraction steps for these samples. Because the age-correction is small, uncertainties in the mineralization age of 100's of Ma would not influence interpretation of these data (full data set available in the appendix).

In contrast, the age-correction for samples AW02-002 and RD03-010A-I with several hundreds ppm K

Table 3
Summary of noble gas and halogen data for fluid inclusions in Mt. Isa dolomite and quartz samples

Sample	Extractions (H=step heat C=crush)	Br/Cl ($\times 10^{-3}$)	I/Cl ($\times 10^{-6}$)	K/Cl	K/Cl max	K ppm	$^{40}Ar/^{36}Ar$ age-corrected	$F^{84}Kr$	$F^{129}Xe$	$Cl/^{36}Ar$ ($\times 10^{6}$)	$^{40}Ar_E/Cl$ ($\times 10^{-6}$)	Salinity, wt.%	$[^{36}Ar_E]$ ppb	$[^{40}Ar_E]$ ppm
				Fluid inc.	Matrix+FI									
		Mean value±standard deviation (1σ)					Max.	Range		Max.	Mean±1σ	Mean and (max) values		
		≤700 °C		≤600 °C	200−1600 °C		200−1600 °C	In vacuo crushing		200−1600 °C				
a. Dolomite alteration														
MG02-324	C 1–6	2.1±0.1	24±2	0.06±0.01	0.07	43	1581±21	0.9–1.0	1.0–2.1	71±4	21±3	26	2.3	3.7
MG02-405	C 1–8	1.53±0.04	186±4	0.086±0.004	0.09	55	7892±104	1.0–1.6	0.9–1.8	91±5	85±2	25	1.7	15
MG02-325A	C 1–4	1.6±0.1	80±3	0.07±0.01	0.08	16	4113±47	1.0–1.2	1.0–1.2	30±2	123±2	20 (26)	4.1 (5.3)	17 (22)
MG02-325B	C 1–7	1.6±0.1	91±5	0.05±0.02	0.07	3	8374±69	0.8–2.4	0.9–3.9	67±3	112±6	20 (26)	1.8 (2.4)	15 (20)
MG02-074	C 1–8	4.3±0.3	40±2	0.07±0.01	0.07	13	1898±14	1.0–1.5	1.3–1.5	29±1	63±9	20 (26)	4.2 (5.5)	8.6 (11)
b. Ore zone silica														
AW02-074	C 1–3 (P2)	12.0±0.1	356±49	0.09±0.02		10	8286±132	0.7–1.9	1.2–4.0	20±1	367±39	16 (20)	4.9 (6.2)	40 (50)
	C 4–8	3.2±0.1	98±6	0.10±0.01	0.29		18,575±908	4.2–4.7	2.9–9.5	45±3	406±10	16 (20)	2.2 (2.7)	44 (56)
	H	3.2±0.3	105±4	0.16±0.07		15	21,176±467	–	–	42±2	492±76	16 (20)	2.3 (2.9)	54 (67)
AW02-076	C 1–8	2.9±0.1	59±2	0.11±0.02	1.1	16	17,824±978	1.0–1.6	2.1–6.6	31±2	553±20	8 (13)	1.6 (2.6)	30 (49)
	H	3.4±0.2	46±12	0.15±0.08		26	15,516±169	–	–	31±2	522±151	8 (13)	1.6 (2.6)	29 (46)
AW03-008	C 1 (P2)	7.2	25			13								
	C 2–8	4.7±0.3	33±6	0.13±0.02	4.1		10,137±312	0.8–1.4	1.0–2.1	21±1	480±86	8 (19)	2.3 (5.6)	26 (62)
	H	3.3±0.3	33±3	0.18±0.1		25	13,033±318	–	–	20±1	600±74	8 (19)	2.5 (5.8)	33 (78)

c. Buck Quartz														
AW03-007	C 1–8	4.7±0.3	24±10	0.10±0.04		18	20,770±2334	0.8–1.4	1.0–9.0	40±5	324±162	3 (19)	~1.5	~21
	H 200 (P3)	1.2	19	–	2.6		667±112	–	–	4.3±0.8	86±15	3 (19)	4.3 (27)	~1.8 (11)
	H	4.9±0.3	16±8	0.11±0.06		51	27,874±555	–	–	37±2	405±353	3 (19)	~1.6	~26
AW03-006	C 1–8	3.7±0.2	26±7	0.11±0.03		14	11,245±115	1.0–1.3	1.0–1.9	23±1	333±111	3 (19)	~2.5	~22
	H 200 (P3)	0.3	–	–	11		–	–	–	–	–	–	–	–
	H	4.1±0.2	24±7	0.07±0.04		75	13,820±430	–	–	29±5	345±129	3 (19)	~2.0	~22
d. Railway fault														
AW02-002a	H	7.7±0.6	12±10		263	819	2491±18	–	–	9.8±0.6	202±43	8 (19)	5.0 (12)	11 (26)
AW02-002b	C+ H	9±3	15±5	0.8±0.1*	551	726	902±11	0.6–1.3	1.2–2.9	4.4±0.3	110±40	8 (19)	11 (27)	6.0 (14)
AW02-002c	H	8.1±0.7	12±3		189	591	1202±29	–	–	5.9±0.4	179±46	8 (19)	8.3 (20)	9.8 (23)
AW02-002d	H	9±1	9±1		136	761	1540±19	–	–	11±1	134±20	8 (19)	4.5 (11)	7.3 (17)
e. Mt. Isa Fault Zone														
RD03-002	C 1–6	8.3±0.6	35±18	0.06±0.01	0.08	5	3027±27	1.0–2.6	1.4–4.0	22±1	146±27	11 (17)	3.1 (4.8)	11 (17)
RD03-010A-I	C 1–9	11±1	47±10	0.31±0.23	8.4	1	542±3	0.8–1.1	0.4–0.8	0.61±0.03	348±78	4	40	9.5
	H	6±3	40±26			9	1667±29	–	–	2.9±0.1	329±239	4	8.5	9.0
RD03-010A-II	C 1–6	29±14	38±29	3.5±1.5 *	155	40	489±4	0.8–3.6	0.1–2.0	0.62±0.03	178±268	6	60	7.3
	H	7±6	156±247			304	392±17	–	–	0.38±0.02	136±30	6	97	5.6

Fluid inclusion K/Cl values for in vacuo crushing and stepped heating (≤600 °C). * The unusually high values determined by in vacuo crushing for AW02-002b and RD02-010A-II are probably attributable to recoil loss of $^{39}Ar_K$ from mineral impurities within these samples into the fluid inclusions, see Kendrick et al. (2006b).

Parts per billion (ppb) ^{36}Ar and parts per million (ppm) $^{40}Ar_E$ are used in preference to $cm^3\ cm^{-3} H_2O$ because they can be calculated from the molar $Cl/^{36}Ar$ and $^{40}Ar_E/Cl$ values and salinity and are independent of fluid density. Based on a fluid density of 1 g cm^{-3}; 1 ppb $^{36}Ar \sim 1.6 \times 10^{-6}$ $cm^3\ cm^{-3}$ H_2O and 1 ppm $^{40}Ar \sim 1.8 \times 10^{-3}$ $cm^3\ cm^{-3}$ H_2O.

Ar concentrations for the high salinity fluid inclusion group in the Buck Quartz Fault samples are estimated using half the maximum salinity value (see text).

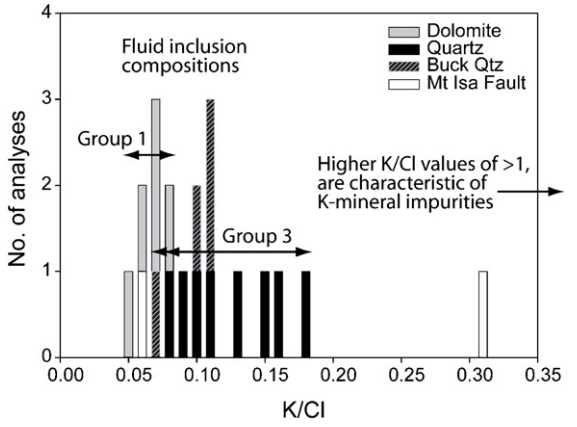

Fig. 7. Mean K/Cl values for Mt. Isa quartz and dolomite samples, in vacuo crushing and stepped heating (<600 °C) data. Two ranges are shown for group 3 fluid inclusions, the first range comprises main-stage quartz samples and the larger range includes the additional Buck Quartz Fault samples.

can be tens of percent and because the K-mineral impurities and fluid inclusions outgas at different temperatures assessment of intra-sample variation is difficult (Kendrick et al., 2006b). Therefore extraction steps with large corrections are omitted from Fig. 8 and the remaining ^{40}Ar data reported for these samples represent an upper limit (Table 3).

5.5. Intra-and inter sample argon variation

The maximum ^{40}Ar/^{36}Ar values determined for the main-stage dolomite (1600–8400) and quartz samples (8300–21,200) are most representative of the fluid inclusions initial composition (Fig. 8 and Table 3). These samples are dominated by a single generation of fluid inclusions with halogen ratios that vary by only 5–10% (Fig. 6). Although a second minor fluid inclusion population was identified in sample AW02-074 (P2 in Fig. 5a), much of the intra-sample ^{40}Ar/^{36}Ar variation is probably explained by an atmospheric Ar contaminant introduced during sample analysis that shifts the fluid inclusion values toward air.

The fluid inclusion $^{40}Ar_E$/Cl values define slopes in Fig. 8 that have atmospheric intercepts and are not altered by the possibility of a modern atmospheric contaminant. Fluid inclusions in the main-stage dolomite and quartz samples exhibit intra-sample $^{40}Ar_E$/Cl variation of 2–30% (Table 3) that is slightly greater, or similar to the variation of Br/Cl and I/Cl in these samples (compare Figs. 6 and 8 plus the standard deviations in Table 3). The group 3 quartz fluid inclusions have mean $^{40}Ar_E$/Cl values of $4–6\times10^{-4}$ that are higher than the mean values of $2–12\times10^{-5}$ for fluid inclusions in dolomite (Table 3 and Fig. 8).

Fluid inclusions in the samples from the Buck Quartz Fault have mean $^{40}Ar_E$/Cl values that are intermediate to the main-stage dolomite and quartz (9×10^{-5} to 3×10^{-4}), but they exhibit 30–90% variation, which like the 50% variation in I/Cl (Fig. 6), suggests the presence of two fluid inclusion groups. The highest salinity fluid inclusions have the highest ^{40}Ar/^{36}Ar values of up to ~28,000 and $^{40}Ar_E$/Cl values similar to group 3 quartz fluid inclusions (Fig. 8). The second group of lower salinity fluid inclusions has ^{40}Ar/^{36}Ar of just 1000–2000 and the lowest $^{40}Ar_E$/Cl values (BQ-2 in Fig. 8). These low values are similar to values determined for fluid inclusions in sample AW02-002 (Table 3), that because of the large age-correction for this sample represent an upper limit (Kendrick et al., 2006b).

5.6. $^{40}Ar_E$ and ^{36}Ar concentration

The fluid inclusion $^{40}Ar_E$ and ^{36}Ar concentrations are determined from the measured $^{40}Ar_E$/Cl and Cl/^{36}Ar values, and the salinities obtained through microthermometry (Section 2.1; Table 3). The variability in fluid inclusion salinity limits the precision of such determinations to the tens of per cent level, which is illustrated by the calculation of Ar concentration for values of

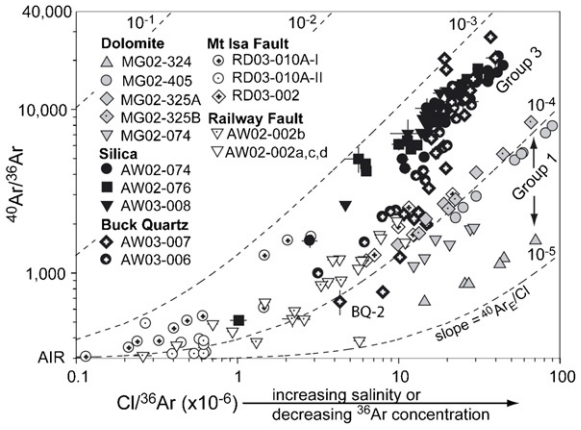

Fig. 8. Log–log ^{40}Ar/^{36}Ar versus Cl/^{36}Ar plot for Mt. Isa quartz and dolomite samples, in vacuo crushing and stepped heating (200–1600 °C) data. Much of the variation in group 1 and group 3 fluid inclusions may be explained by a modern atmospheric Ar contaminant. However, the variable fluid inclusion $^{40}Ar_E$/Cl values in samples from the Buck Quartz Fault indicate the presence of two fluid inclusion groups. The first fluid inclusion group, with the highest ^{40}Ar/^{36}Ar values is similar to the main-stage quartz fluid inclusions (group 3). The second fluid inclusion group (BQ-2) with lower $^{40}Ar_E$/Cl and ^{40}Ar/^{36}Ar values is similar to fluid inclusions in the Railway Fault samples.

maximum as well as mean salinity, in most cases (Table 3). However, representative Ar concentrations for the higher salinity fluid inclusions in the Buck Quartz Fault samples are estimated using half the maximum salinity value (Table 3). This is necessary because the Buck Quartz Fault samples contain two groups of fluid inclusion (group 3 and BQ-2) and the mean salinity value is not representative of the high salinity fluid inclusion group (see Fig. 4). The effect of the possible atmospheric Ar contaminant is minimized by calculating ^{36}Ar concentration from the maximum Cl/^{36}Ar value measured for each sample, but the ^{36}Ar concentrations are nonetheless upper limits.

Fluid inclusion $^{40}Ar_E$ concentrations are 26–78 ppm in the main-stage quartz samples (group 3) and 4–22 ppm in the dolomite samples (Fig. 9; Table 3). The ^{36}Ar concentration is negatively correlated with ^{40}Ar/^{36}Ar across the sample groups (Fig. 9). The lowest values of ~1.5 ppb ^{36}Ar are determined for fluid inclusions in samples from the Buck Quartz Fault and the main-stage quartz, which have the highest ^{40}Ar/^{36}Ar values of up to 28,000 (Table 3). Fluid inclusions in some of the main-stage dolomite samples have similar ^{36}Ar concentrations that are within error or close to Air Saturated Water (ASW = 1.3–2.7 ppb) and ^{40}Ar/^{36}Ar exhibits a weakly

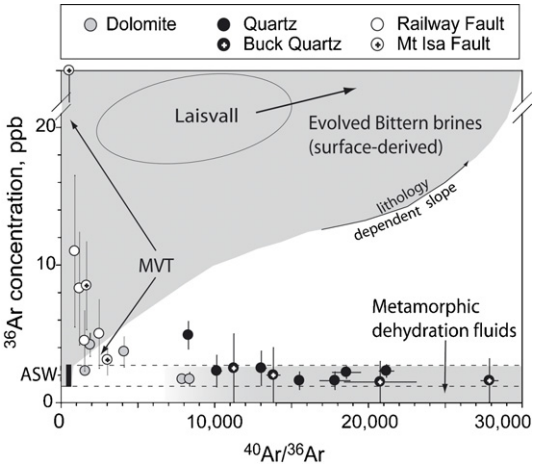

Fig. 9. ^{36}Ar concentration versus maximum ^{40}Ar/^{36}Ar for Mt Isa quartz and dolomite samples, in vacuo crushing and stepped heating (200–1600 °C) data. The compositions of deeply derived metamorphic fluids, air saturated water (ASW) and surface-derived bittern brines are shown for reference (discussed fully in Section 6). Mean ^{36}Ar concentration values are given for samples dominated by a single generation of fluid inclusions with uncertainties in ^{36}Ar concentration reflecting fluid inclusion salinity variations as follows: dolomite 10–20%; silica 20–50%, Railway Fault 50%; Mt Isa Fault 20% (Table 3). The Buck Quartz Fault samples include two groups of fluid inclusion, and in this case the ^{36}Ar concentrations of the highest salinity fluid inclusions are estimated as half the maximum value with the error bars equal to 100%.

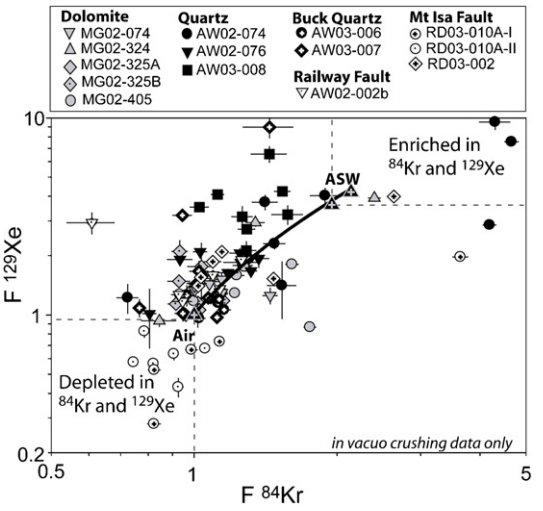

Fig. 10. Log–log F^{84}Kr versus F^{129}Xe for data obtained by *in vacuo* crushing. The fractionation values (*F*-values) define a mixing line between air (*F* = 1) and air saturated water (ASW = meteoric water and seawater). The fractionation values are defined as; $FX = (X/^{36}Ar)_{sample}/(X/^{36}Ar)_{air}$; reference values in Ozima and Podosek (2002). Nb—slightly more data points lie above than beneath the mixing line, and stepped heating analyses are ^{129}Xe-enriched relative to in vacuo crushing analyses (appendix). The ^{129}Xe enrichment is explained by a fissionogenic component formed from trace U in the quartz matrixes. The fissionogenic Xe isotopes remain poorly resolved and close to the detection limit so inferred sub-ppb to ppb U abundances are unreported.

negative correlation with ^{36}Ar concentration in this sample group (Fig. 9). The ^{36}Ar concentration is highest in fluid inclusions within samples from the Railway and Mt Isa Faults with the lowest ^{40}Ar/^{36}Ar values. The maximum ^{36}Ar concentration of ~100 ppb, determined for fluid inclusions in sample RD03-010A-II, is almost two orders of magnitude higher than ASW (Fig. 10; Table 3).

5.7. Argon versus krypton, xenon and the halogens

Fluid inclusions in the majority of main-stage dolomite and quartz samples and the samples from the Buck Quartz plus Railway Faults have noble gas fractionation values (F^{84}Kr and F^{129}Xe)[2] that cluster around the mixing line between air and ASW (Fig. 10). Mixing between air and ASW is consistent with some of the fluid inclusion analyses having been affected by a modern atmospheric Ar (plus Kr and Xe) contaminant.

[2] Noble gas fractionation values (*F*-values) indicate fractionation relative to ^{36}Ar in air such that: $FX = (X/^{36}Ar)_{sample}/(X/^{36}Ar)_{air}$. Air has an *F* value of 1, and *F*-values of less than one indicate depletion in the heavy noble gases ^{84}Kr and ^{129}Xe relative to ^{36}Ar in air.

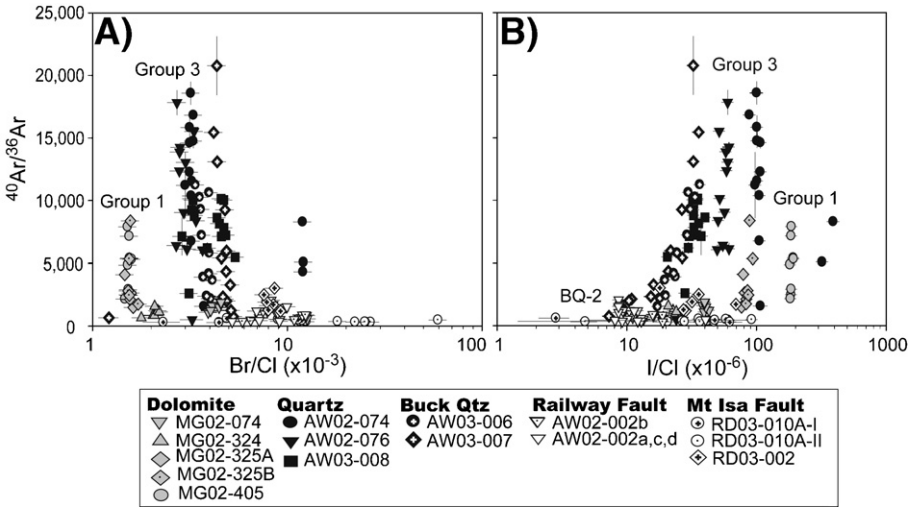

Fig. 11. Argon versus halogen plots for Mt Isa quartz and dolomite samples, in vacuo crushing and stepped heating (200–700 °C) data. (A) Br/Cl vs. $^{40}Ar/^{36}Ar$, (B) I/Cl vs. $^{40}Ar/^{36}Ar$. Note trend in data from the Buck Quartz Fault samples from a low I/Cl and low $^{40}Ar/^{36}Ar$ fluid inclusion end-member (BQ-2) up to a high I/Cl and $^{40}Ar/^{36}Ar$ end-member that is similar to group 3.

Only the Mt Isa Fault samples RD03-010A-I and -II contain fluid inclusions that yield an appreciable number of fractionation values that are consistently outside the air-ASW range (Fig. 10). The low fractionation values together with the much greater than ASW ^{36}Ar concentrations in these samples (Fig. 9), indicate noble gas enrichment on the order $^{36}Ar > ^{84}Kr > ^{129}Xe$. This is yet another parameter that distinguishes fluids in the Mt Isa Fault from those involved in mineralization.

The majority of quartz and dolomite samples contain fluid inclusions with $^{40}Ar/^{36}Ar$ values that vary independently of Br/Cl and I/Cl (Fig. 11), consistent with some of the $^{40}Ar/^{36}Ar$ variation being caused by the presence of an atmospheric Ar contaminant. An exception is the correlation of fluid inclusion $^{40}Ar/^{36}Ar$ and I/Cl values in the samples from the Buck Quartz Fault. These samples contain two fluid inclusion groups the composition of which are summarized together with the composition of main-stage dolomite and quartz fluid inclusions in Table 4.

6. Bittern brines versus 'metamorphic' fluids

The fluid inclusions trapped in main-stage quartz and dolomite, and the regional fault samples, have complex origins that cannot be resolved from the halogen data alone. The high Br/Cl and I/Cl values preclude evaporite dissolution which leads to low values (Table 4; Holser, 1979), but are typical of bittern brine sedimentary formation waters that acquire salinity by sub-aerial evaporation and some high grade metamorphic fluids (Fig. 6; Zherebtsova and Volkova, 1966; Carpenter et al., 1974; Walter et al., 1990; Heinrich et al., 1993; Svensen et al., 2001; Kendrick et al., 2002a,b). Similarly, quartz fluid inclusion salinities of less than ~20 wt.%, could be explained by either a metamorphic origin or by the variable dilution of a bittern brine with starting salinity of ~26 wt.% (Table 4).

To complicate matters further, both alternatives are geologically realistic. The late-Isan mineralisation event is favoured to have had similar timing to post-peak metamorphism of the Sybella Batholith at ~1530 Ma (e.g. Perkins, 1984; Swager, 1985; Bell et al., 1988; Connors and Page, 1995; Perkins et al., 1999), implying the possible availability of metamorphic dehydration fluids. The Kennedy Siltstone preserves halite pseudomorphs and stromatilites that provide evidence for shallow water evaporitic environments during deposition of the Mt Isa Group (Neudert and Russel, 1981). In addition, similar evaporitic environments may have existed above the present erosion level at the time of mineralization, implying the possible availability of bittern brines.

In an effort to resolve these alternative fluid origins, we have evaluated the Ar isotope composition and salinity of evolved bittern brine sedimentary formation waters and metamorphic fluids:

6.1. Bittern brines

Bittern brines with greater than seawater Br/Cl values form by the sub-aerial evaporation of seawater (or lake water) beyond the point of halite saturation (~26-30 wt.%) and therefore have an initially atmospheric $^{40}Ar/^{36}Ar$ value (modern value=295.5) and a salinity of ~26–

30 wt.% (Table 4). Due to their high salinity and the 'salting out' effect they are expected to have lower than seawater ^{36}Ar concentrations of <1.3 ppb (Smith and Kennedy, 1983; Ozima and Podosek, 2002).

Hydrothermal fluids involved in MVT ore deposits originated as sedimentary formation waters and the majority have higher than seawater Br/Cl values that are typical of a bittern brine origin (e.g. Kesler et al., 1995; Viets et al., 1996; Kendrick et al., 2002a,b). However, at the 1–2 km depth of mineralization, MVT ore fluids have elevated $^{40}Ar/^{36}Ar$ values that are typically in the range 300–1500 providing evidence for excess $^{40}Ar_E$ acquisition during low temperature (<200 °C) fluid–rock interaction (Kelley et al., 1986; Böhlke and Irwin, 1992a; Turner and Bannon, 1992; Kendrick et al., 2002a,b).

Furthermore, the majority of MVT ore fluids studied to date have elevated ^{36}Ar concentrations of ~3–27 ppb that are higher than expected for Air Saturated Water (ASW; meteoric or seawater=1.3–2.7 ppb), and much higher than expected for air saturated bittern brines (Kelley et al., 1986; Turner and Bannon, 1992; Kendrick et al., 2002a,b). In addition, similar ore fluids in the Laisvall sandstone-hosted Pb–Zn deposit have even higher ^{36}Ar concentrations of up to ~40 ppb and $^{40}Ar/^{36}Ar$ values of up to ~16,000 that are an order of magnitude higher than is typical for MVT ore fluids (Kendrick et al., 2005).

6.1.1. ^{36}Ar acquisition

The greater than ASW ^{36}Ar concentrations of ore fluids that originated as sedimentary formation waters have previously been interpreted with caution. It is possible that ^{36}Ar was introduced as a modern atmospheric contaminant during analysis and that the real fluid ^{36}Ar concentration was lower (Turner and Bannon, 1992; Kendrick et al., 2002a,b). However, we argue that the elevated ^{36}Ar concentrations are expected in surface-derived sedimentary formation waters that have acquired a few ppm $^{40}Ar_E$ from aquifer rocks. Aquifer rocks have finite $^{40}Ar/^{36}Ar$ values and fluid acquisition of $^{40}Ar_E$ will therefore be accompanied by 'excess' ^{36}Ar (Fig. 12).

If ^{36}Ar is acquired together with $^{40}Ar_E$ from aquifer rocks, as suggested (Fig. 12), the ^{36}Ar concentration of a surface-derived ore fluid can be predicted from an Ar reservoir mixing model (Fig. 12) using Eq. (1):

$$[^{36}\text{Ar ppb}]_{Fm} = [^{36}\text{Ar ppb}]_{F_1} + \left(\frac{^{40}Ar/^{36}Ar_{Fm} - ^{40}Ar/^{36}Ar_{F_1}}{^{40}Ar/^{36}Ar_R - ^{40}Ar/^{36}Ar_{Fm}}\right) \cdot [^{36}\text{Ar ppb}]_{F_1} \quad (1)$$

Where Fm=the mineralizing fluid; F1=the initial surface-derived fluid; R=aquifer rock; and $\frac{^{40}Ar/^{36}Ar_{Fm} - ^{40}Ar/^{36}Ar_{F1}}{^{40}Ar/^{36}Ar_R - ^{40}Ar/^{36}Ar_{Fm}}$ gives the ratio of Ar in the mineralizing fluid sourced from the aquifer rocks relative to Ar originally present in the surface-derived fluid (R/F1).

The implication is that, in the absence of phase separation, the ^{36}Ar concentration in surface-derived fluids will exhibit a positive correlation with $^{40}Ar/^{36}Ar$, as observed between Laisvall and other MVT ore fluids (Fig. 9; Turner and Bannon, 1992; Kendrick et al., 2002a,b, 2005). The slope of this correlation is lithology dependent and will approach infinity as the $^{40}Ar/^{36}Ar$ value of the fluid approaches the $^{40}Ar/^{36}Ar$ value of the aquifer lithology (Eq. (1)). Furthermore, where fluids interact with several lithologies with diverse $^{40}Ar/^{36}Ar$ values, the slope could appear uneven (e.g. Fig. 9). The intercept of the slope is inferred to be close to the ^{36}Ar concentration of ASW (1.3–2.7 ppb), but it could be lower in a bittern brine, due to the salting out effect, or higher if air bubbles are entrained in the fluid (e.g. Ozima and Podosek, 2002). As a result, the ^{36}Ar concentration is only a useful indicator of surface recharge conditions in palaeo-fluids with low $^{40}Ar/^{36}Ar$ values that have not undergone extensive fluid–rock interaction (cf. Böhlke and Irwin, 1992a). In other circumstances the ^{36}Ar concentration, together with the $^{40}Ar/^{36}Ar$ value, provides useful information on the extent of fluid–rock interaction or the nature of the aquifer reservoir from which Ar has been derived (Eq. (1)). In the Mt Isa case, the lack of a positive correlation between ^{36}Ar concentration and $^{40}Ar/^{36}Ar$ (Fig. 9) suggests that the fluid inclusions in the different sample groups at Mt Isa did not all originate at the surface.

6.2. Metamorphic fluid

In contrast to surface-derived fluids, a metamorphic fluid derived from initially deep-crustal rocks will have $^{40}Ar/^{36}Ar$, $^{40}Ar_E/Cl$, salinity, ^{36}Ar and $^{40}Ar_E$ concentrations determined by the $Cl/^{36}Ar/^{40}Ar/OH$ ratio in the devolatilising source region and subsequent fluid–rock interactions. Based on the simplifying assumption of quantitative devolatilisation of the source region, or that OH, Cl and Ar are devolatilised with similar efficiencies, the Ar isotope characteristics and salinity of a metamorphic fluid can be estimated as follows:

$$^{36}\text{Ar ppb} \approx \frac{^{36}\text{Ar mol g}^{-1^{-1}}}{\text{OH mol g}^{-1}} \cdot \frac{36}{17} \cdot 10^9 \quad (2)$$

Table 4
Fluid types detected in the mine area with interpreted significance for mineralization/alteration

Sample	Salinity wt. %	Br/Cl ($\times 10^{-3}$)	I/Cl ($\times 10^{-6}$)	K/Cl[a]	$^{40}Ar/^{36}Ar$ [b]	[^{36}Ar], ppb	[$^{40}Ar_E$], ppm	Notes
Fluid 1: Deeply derived metamorphic fluid (Group 3 fluid inclusions)								
Main-stage quartz and Buck Quartz (group 3)	8–20	2.9–4.9	33–105	0.07–0.18	8300–28,000	1.6 to ~3	11–78	The metamorphic fluid end-member is best represented by the fluids with the highest $^{40}Ar/^{36}Ar$ and Br/Cl values. Salinity is lower than halite-saturated seawater.
Fluid 2: Surface-derived bittern brine sedimentary formation water (Group 1 fluid inclusions)								
Main-stage dolomite (group 1)	18–26	1.5–4.3	24–187	0.05–0.09	1600–8400	1.7–5.5	3.7–22	The bittern brine fluid end-member is best represented by the fluids with the lowest $^{40}Ar/^{36}Ar$ and Br/Cl values. Salinity is close to halite-saturated seawater, but I/Cl is enriched relative to the seawater evaporation trajectory reflecting interaction with organic-rich sedimentary rocks (Fig. 6).
Fluid 3: Surface-derived bittern brine sedimentary formation water								
Railway Fault and Buck Quartz (BQ-2)	1–19	7–9	9–15	?	~1000–2500	4.5–27	6.0–23	The low $^{40}Ar/^{36}Ar$ values and high ^{36}Ar concentrations plus high but variable Br/Cl values are typical of bittern brines. The low salinity indicates post-evaporation dilution of the bittern brine, and the high I/Cl value reflects interaction with organic–rich sedimentary rocks.

Reference values									
Meteoric water		~0				295.5	1.6–2.7	~0	Modern day values
Seawater		3.5	1.54	0.86	0.02	295.5	1.3–2.0	~0	Modern day values
Sed. Fm	Halite Diss.	1–70	~0.1	<0.86	variable	Low to High*	~ASW and higher*	Low to High*	Bittern brines have salinity close to the point of halite saturation, halite dissolution can result in higher salinities. $^{40}Ar_E$, ^{36}Ar and I are acquired by fluid–rock interaction in the sub-surface. *Asterisk indicates evolved fluids.
Water	Bittern Brine	~26–30	>1.54	≫0.86					
Metamorphic fluid		variable	variable	variable	variable	High*	≤ASW*	High*	Composition is determined by source region, but the salinity, Br/Cl and I/Cl values may be increased during retrograde hydration reactions. *Astersk indicates probable values for old crystalline rocks.

Value ranges represent the sample mean values summarised in Table 3.

Mineralisation/alteration are interpreted to result from mixing of fluids 1 and 2. The alteration and mineralization may have terminated when fluid 3 entered the mine area along the post-D_3 Buck Quartz Fault.

Reference values in Zherebtsova and Volkova (1966), Holser (1979), McCaffrey et al. (1986), Böhlke and Irwin (1992a), Ozima and Podosek (2002), see discussion in Section 6.

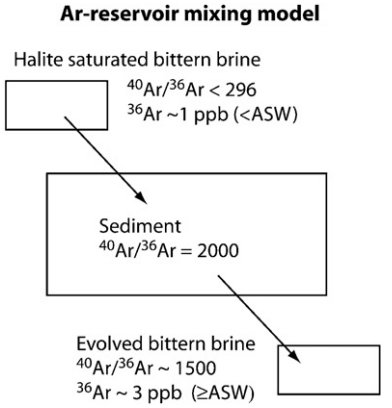

Fig. 12. Unlike stable isotopes (O, H or C), Ar-isotopes are strongly incompatible, meaning they are lost to the fluid phase during water–rock interaction (above the Ar closure temperature) and isotope exchange does not take place. As a result, the fluid ^{36}Ar concentration will be increased together with the $^{40}Ar/^{36}Ar$ value and the Ar-isotope signature is added to and not reset, see text.

$$^{40}Ar_E\,ppm \approx \frac{(K\ mol\ g^{-1})\cdot(^{40}K/K)\cdot(\lambda_e/\lambda)\cdot(e^{\lambda t}-e^{\lambda t_o})}{OH\ mol\ g^{-1}}\cdot\frac{40}{17}\cdot 10^6 \quad (3)$$

$$wt.\%\ NaCl\ eq. \approx \frac{Cl\ mol\ g^{-1}}{OH\ mol\ g^{-1}}\cdot\frac{58.5}{17}\cdot 100 \quad (4)$$

$$\frac{^{40}Ar}{^{36}Ar} = \frac{(^{36}Ar\ mol\ g^{-1^{-1}}\cdot 295.5)+(K\ mol\ g^{-1})\cdot(^{40}K/K)\cdot(\lambda_e/\lambda)\cdot(e^{\lambda t}-e^{\lambda t_o})}{^{36}Ar\ mol\ g^{-1}} \quad (5)$$

$$^{40}\frac{Ar_E}{Cl} = \frac{(K\ mol\ g^{-1})\cdot(^{40}K/K)\cdot(\lambda_e/\lambda)\cdot(e^{\lambda t}-e^{\lambda t_o})}{Cl\ mol\ g^{-1}} \quad (6)$$

Where the concentrations in mol g^{-1} refer to the whole rock in the source region; t is the age of the rock and t_o is the time of leaching in years (assumed to be the mineralization age of ~1530 Ma in this case) and the constants are $^{40}K/K = 0.00012$; $\lambda_e = 0.581\times10^{-10}$ year^{-1}, $\lambda = 5.543\times10^{-10}$ year^{1}. Eqs. (3), (5) and (6) represent modified forms of the K–Ar decay equation and Eq. (6) is after Turner and Bannon (1992).

6.2.1. General characteristics

Based on the mean whole rock ^{36}Ar concentration of crystalline basement rocks in Germany (~2×10^{-13} mol g^{-1}; Drescher et al., 1998), quantitative devolatilisation of a source region comprising 100% Mg-rich biotite (with an OH^- concentration of ~5×10^{-3} mol g^{-1}) would yield a metamorphic fluid with ~0.08 ppb ^{36}Ar. If hydrous phases comprised only five percent of the rock giving an OH concentration of ~2.5×10^{-4} mol g^{-1}, the ^{36}Ar concentration would be increased to ~1.6 ppb (Eq. (2); Fig. 13A). The corresponding salinity of these fluids would be ~0.2–4 or ~1–20 wt.% NaCl eq., if sourced from rocks with realistic Cl concentrations of either ~100 ppm or ~500 ppm, respectively (Eq. (4); Fig. 13B).

In general terms deeply derived metamorphic fluids are expected to have low ^{36}Ar concentrations of less than or equal to Air Saturated Water (ASW) and low salinities, but both will be highly variable depending upon the source region and could be increased by retrograde hydration reactions. Significantly greater than ASW ^{36}Ar concentrations (>1.3–2.7 ppb) could probably only result from devolatilisation of sedimentary rock source regions that are enriched in ^{36}Ar (Fig. 13A; Ozima and Podosek, 2002), and are in any case likely to contain pore fluids prior to devolatilisation. The biggest difference to surface-derived fluids is that the ^{36}Ar concentration should not be correlated with $^{40}Ar/^{36}Ar$ (Fig. 9; Eqs. (2) and (5)).

6.2.2. Application to Mt Isa

Limits can be placed on the $^{40}Ar/^{36}Ar$, $^{40}Ar_E/Cl$ and $^{40}Ar_E$ values expected for fluids evolved from the different lithologies at Mt Isa, based on the K content and ages of these units, if we make some simplifying assumptions about the initial Cl plus ^{36}Ar concentration and the degassing history of these rocks (Eqs. (3), (4) and (6)).

The ~1655 Ma Urquhart Shale (Page et al., 2000) would have had a maximum $^{40}Ar/^{36}Ar$ value of ~4000–5000 at the time of mineralization (~1530 Ma), based on a K content of 3–3.7 wt.% (Neudert, 1983; McGoldrick, 1986; Waring, 1990), a maximum detrital age of ~1830 Ma, and an initial ^{36}Ar concentration of 10^{-12} mol g^{-1} which is in the range determined for sedimentary rocks (Ozima and Podosek, 2002). Although possible changes in Ar concentration during D_2 metamorphism have not been accounted for, the assumed detrital age of ~1830 Ma suggests that the calculated value represents an upper limit. Therefore, sedimentary rocks similar to the Urqhuart Shale are extremely unlikely to have been the source of high $^{40}Ar/^{36}Ar$ fluid inclusions in our samples.

Similar calculations do not allow conclusive discrimination of potential source rocks such as the unaltered Eastern Creek Volcanics (ECV) from the Barramundi Basement. The unaltered 1780 Ma ECV (Farquharson and Richards, 1974; Neumann et al., in press) have 1.2–1.7 wt.% K_2O (Hannan et al., 1993; Heinrich et al., 1995) equivalent to <1.5 wt.% K. The older, 1870 Ma Barramundi Basement is felsic-rich (Page and Williams, 1988; O'Dea et al., 1997) and in the following calculations is assumed to have a K concentration of 3 wt.%, representative for granitic rocks. Together with

reasonable ranges of ^{36}Ar concentration, these values indicate that it is theoretically possible to extract a metamorphic fluid with a $^{40}Ar/^{36}Ar$ value of 10,000–28,000 and a ^{36}Ar concentration of ~1–3 ppb from either lithology (Fig. 13A). However, the highest $^{40}Ar/^{36}Ar$ values could only be achieved in the ECV if they were depleted in ^{36}Ar relative to the mean for crystalline rocks in Germany (Fig. 13A; Drescher et al., 1998).

Similarly, based on reasonable ranges in Cl concentration, the maximum fluid $^{40}Ar_E/Cl$ values of ~3–10×10^{-4} (mostly $<8\times10^{-4}$) and salinities of 10–20 wt. % NaCl eq. (Table 3) could be attained by devolatilisation of either lithology (Eq. (6); Fig. 13B). However, to account for the full range of $^{40}Ar_E/Cl$ values, the ECV would need to be enriched in Cl relative to the mean for tholeiitic oceanic crust (Fig. 13B; Schilling et al., 1978).

Considering the uncertainties involved, the combined estimates of fluid $^{40}Ar/^{36}Ar$, ^{36}Ar concentration, $^{40}Ar_E/Cl$ and salinity, obtained using realistic ages and whole rock K, Cl plus ^{36}Ar concentrations, match the range of values measured in quartz fluid inclusions remarkably well (compare Table 3 with Fig. 13). This good match between the modeled values and the values measured in quartz fluid inclusions supports the interpretation of a metamorphic fluid origin and indicates that metamorphic fluids may have been derived from both the ECV and the Barramundi Basement.

The ECV has been suggested as a fluid source rock previously (Hannan et al., 1993) and it is favoured as a source of Cu (Hannan et al., 1993; Heinrich et al., 1995). However, at least some involvement of the Barramundi Basement is favoured by the noble gas data because the Barramundi Basement is most likely to have had the highest $^{40}Ar/^{36}Ar$ values and a range of $^{40}Ar_E/Cl$ values that overlap those measured in the quartz fluid inclusions; based on the mean concentrations of ^{36}Ar and Cl in the relevant rock types (Fig. 13). Furthermore, a

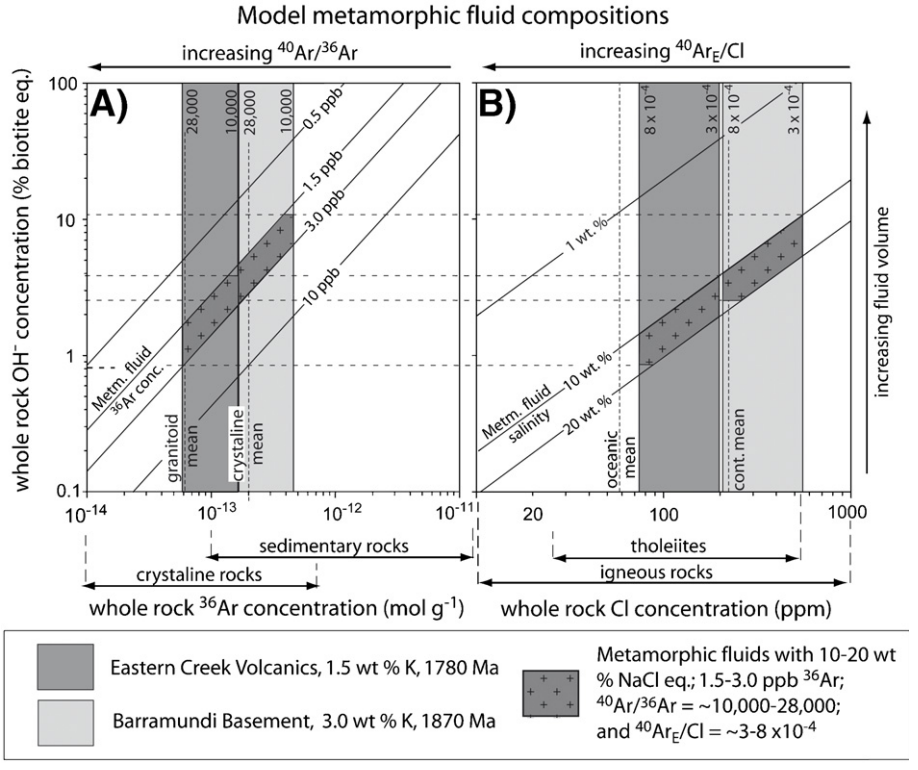

Fig. 13. Combined diagrams showing the model (A) ^{36}Ar concentration of a metamorphic fluid as a function of whole rock OH and ^{36}Ar concentration and (B) the salinity of a metamorphic fluid as a function of whole rock OH and Cl concentration. The fluid $^{40}Ar/^{36}Ar$ and $^{40}Ar_E/Cl$ values are determined by the rocks' K content, age, ^{36}Ar and Cl concentration, and are independent of the OH concentration (vertical lines). The respective ranges of whole rock ^{36}Ar and Cl concentrations that could have produced fluids with the measured range of $^{40}Ar/^{36}Ar$ and $^{40}Ar_E/Cl$ values are shown as vertical boxes for the ECV and Barramundi Basement. Whole rock OH concentration, is expressed as percentage biotite equivalent, where a rock comprising 100% Mg-rich biotite has an OH concentration of 5×10^{-3} mol g^{-1}. The ranges of whole rock ^{36}Ar and Cl concentrations are given beneath the x-axis with various mean values indicated by dashed vertical lines (Schilling et al., 1978; Allegre et al., 1987; Shinonaga et al., 1994; Drescher et al., 1998). Dashed horizontal lines are to guide the eye only.

greater volume of fluid could be derived from the Barramundi Basement because the Barramundi Basement is more voluminous than the ECV (being open to depth) and its felsic-rich mineralogy would probably have been richer in hydrous minerals (cf. *y*-axis Fig. 13).

7. Fluid mixing versus wall–rock interaction

7.1. Fluid end-members

The Ar isotope composition of fluid inclusions in the main-stage quartz and Buck Quartz Fault samples with $^{40}Ar/^{36}Ar$ of ~10,000 to 28,000 and uncorrelated ^{36}Ar concentrations of ~1–3 ppb are most easily explained by a deep crustal metamorphic fluid origin (Section 6; Figs. 9 and 13). These fluids have salinities of <20 wt.% NaCl eq. and the high Br/Cl and I/Cl values may reflect either the composition of the metamorphic source region or retrograde hydration reactions in a rock-buffered system with very low water–rock ratio (Svensen et al., 2001).

In contrast, fluid inclusions in the dolomite samples have lower maximum $^{40}Ar/^{36}Ar$ values, with the lowest values of 1600–1900 being similar to those obtained in sedimentary formation waters (Tables 3 and 4; Böhlke and Irwin, 1992a; Turner and Bannon, 1992; Kendrick et al., 2002a,b). Therefore, the high Br/Cl values in the dolomite fluid inclusions could reflect acquisition of salinity by subaerial evaporation of surface water beyond the point of halite saturation. Such a bittern brine origin is compatible with the high salinity of the group 1 dolomite fluid inclusions that remain close to halite saturation (~26 wt.%; Table 3). However, the poorly defined negative correlation between $^{40}Ar/^{36}Ar$ and ^{36}Ar concentration (Fig. 9) is the opposite to that expected in surface-derived fluids that have interacted with high $^{40}Ar/^{36}Ar$ rocks (Section 6.1). This feature of the data, together with the total variation in Br/Cl and I/Cl may be explained by mixing a surface-derived bittern brine with a component of the deeply derived metamorphic fluid previously identified.

7.1.1. Regional faults

The high ^{36}Ar concentrations and $^{40}Ar/^{36}Ar$ values of ~1000–2500 (Table 3; Fig. 9), in fluid inclusions contained in the Railway and Mt Isa Fault samples are similar to those expected for a fluid with an exclusively sedimentary formation water origin (but see below).

The fluid inclusion Br/Cl values for the Railway Fault samples are in the range expected for the evaporation of seawater but are significantly higher than values obtained from fluid inclusions in the dolomite samples, thus suggesting an independent origin. The fluid inclusions in the Railway Fault have salinities of 4–19 wt.% NaCl eq. that are lower than the dolomite fluid inclusions (Table 3). These salinities are also lower than the point of halite saturation (~26 wt.%), that characterise bittern brines formed by evaporation beyond the point of halite saturation (Table 4), and the low salinities therefore indicate brine dilution prior to fluid trapping.

The Railway Fault fluid inclusions are similar to the second group of fluid inclusions (BQ-2) contained within samples from the Buck Quartz Fault, which otherwise contain fluid inclusions similar to group 3 main-stage quartz (Figs. 4, 6, 8 and 11 and Table 4). The existence of two groups of primary fluid inclusion within samples from the Buck Quartz Fault provide direct (intra-sample) evidence for the close timing of different fluid flow events within a single fault at Mt Isa and support the concept of fluid mixing.

7.2. Limited potential of fluid–rock interaction

The variable composition of the metamorphic fluid is probably partially attributable to the variable nature of the source region (Fig. 13), but retrograde hydration reactions could further modify the salinity, Br/Cl and I/Cl values close to the source region where low water-rock ratios predominate (Svensen et al., 2001). However, Br and Cl are minor constituents of silicate minerals and in fluid buffered hydrothermal systems and in the absence of halite, such as at the site of mineralization, they are believed to behave in a conservative manner (e.g. Hanor, 1994; Worden, 1996). Therefore, the different Br/Cl values of fluid inclusions with moderately high salinity (Table 3) and a preferred bittern brine origin in samples from the main-stage dolomite (group 1) and the Railway Fault, are unlikely to be explained by fluid–rock interaction, and their independent origins are supported.

Fluid interaction with sedimentary rocks has the potential to alter the I/Cl and $^{40}Ar/^{36}Ar$ values of the fluid. Organic-rich sedimentary rocks are I-rich (Worden, 1996) and will have lower $^{40}Ar/^{36}Ar$ values than the metamorphic source region (Section 6.2.2). Therefore a metamorphic fluid that interacted with sedimentary rocks could acquire a low $^{40}Ar/^{36}Ar$ value, a high ^{36}Ar concentration and an elevated I/Cl value. Therefore if all the fluids had a metamorphic origin, such fluid–rock interactions provide an alternative explanation (to fluid mixing) for the negative correlation between $^{40}Ar/^{36}Ar$ and ^{36}Ar concentration seen between the sample groups (Fig. 9). However, the total variation in fluid inclusion noble gas and halogen compositions seen between different sample groups (Figs. 5–11; Table 3) is unlikely to be explained by fluid–rock interaction alone, but is easily explained by mixing independently derived fluid types.

7.2.1. Mt Isa fault

In contrast, samples from the Mt Isa Fault contain fluid inclusions with Br/Cl values of up to $\sim 30 \times 10^{-3}$, and it is possible that the highest Br/Cl values in these low salinity fluids ~6 wt.% NaCl eq. are explained by a metamorphic origin. If hydrous minerals formed during retrograde hydration reactions take up OH and Cl preferentially, relative to Br and I (e.g. Svensen et al., 2001), they may be able to produce much higher salinities and Br/Cl values than are attained during seawater evaporation (Fig. 6; Zherebtsova and Volkova, 1966).

Fluid inclusions in the Mt Isa Fault samples have low $^{40}Ar/^{36}Ar$ values and exceptionally high ^{36}Ar concentrations of up to ~100 ppb (Fig. 9). If the salinity of these fluids had a metamorphic origin, the enrichment of these fluid inclusions in ^{36}Ar is consistent with Ar acquisition from either sedimentary rocks with a low $^{40}Ar/^{36}Ar$ value, or dilution by a negligibly saline sedimentary formation water. The fluid history recorded by fluid inclusions in the Mt Isa Fault samples appear to be unrelated to fluid histories recorded by fluid inclusions in the other sample groups.

8. Summary of genetic model

The proposed metamorphic origin for group 3 fluid inclusions trapped in main-stage quartz and Buck Quartz Fault samples, is compatible with the syn-D_3 timing of mineralization that may have been synchronous with post-D_2 metamorphism of the nearby Sybella Batholith at ~1530 Ma (Perkins, 1984; Swager, 1985; Bell et al., 1988; Connors and Page, 1995; Perkins et al., 1999; see Table 1). A metamorphic origin is also suggested by the elemental and stable isotope geochemistry of the variably altered Eastern Creek Volcanics (Hannan et al., 1993) that were probably an important source of copper (e.g. Heinrich et al., 1995).

The main-stage dolomite fluid inclusions better preserve fluids with a bittern brine origin, and are inferred to contain only a minor metamorphic component. Independent origins for fluid inclusions in main-stage quartz and dolomite are compatible with the fluid inclusion and stable isotope (C, O, H) data for these alteration phases (Heinrich et al., 1989, 1993, 1995). Furthermore the involvement of bittern brines formed by sub-aerial evaporation of a surface water beyond the point of halite saturation, is compatible with the possible involvement of seawater sulphate, as indicated by S-isotope data (Andrew et al., 1989; Hannan et al., 1993).

The ultimate source of deep fluids could have been either within the Eastern Creek Volcanics at the greenschist-amphibolite facies transition (Hannan et al., 1993), but an even deeper source in the Barramundi Basement (at the amphibolite-granulite facies transition?) is arguably favoured by the Ar data (Fig. 13). Because the metamorphic fluid was evolved at very low water-rock ratio (Fig. 13) and a substantial volume of fluid is required for mineralization, it is implied that fluid was sourced from a large volume of crust. As proposed by Bell et al. (1988), the relatively narrow D_3 strain zones may have been responsible for efficiently focusing this deeply-derived fluid into the site of mineralisation.

Fluid mixing may have proceeded by either displacement of a pore fluid or by active convection (Fig. 14). Dolomite is inferred to have precipitated from the carbonate-rich bittern brine sedimentary formation water pore fluid. The outward displacement of this fluid may have resulted in the changed physio-chemical conditions that caused dolomite precipitation. The outward displacement of the pore fluid may explain the dominance of dolomite in the outer parts of the silica–dolomite alteration halo, quartz veins overprinted the early dolomite as the mineralizing system evolved and became dominated by the silica saturated, deeply derived, metamorphic fluid.

Alternatively, the multiple stages of dolomite and quartz veining and the potentially protracted nature of the mineralization event may require a longer lived active-mixing model. Mixing between a downwardly convecting bittern brine with an ascending metamorphic fluid might have occurred at Mt Isa because the Paroo Fault was reactivated during D_3 deformation (Bell et al., 1988). This reactivation provided an accommodation space in which fluids could mix and subsequent over pressuring lead to brecciation (e.g. Bell et al., 1988; Heinrich et al., 1989).

There is considerable uncertainty regarding the absolute duration of the mineralization process. It is possible that introduction of a low salinity, diluted bittern brine, preserved in fluid inclusions within the post-D_3 Railway and Buck Quartz Faults represented the termination of mineralization. However, main-stage group 3 fluid inclusions are also preserved within the Buck Quartz Fault samples which together with the many post-D_3 chalcopyrite-bearing quartz veins (Perkins, 1984) could indicate that deeply-derived metamorphic fluids where introduced multiple times up until the late-orogenic stage of brittle wrenching (Section 2).

9. Conclusions

- Deeply derived metamorphic fluids are characterized by uncorrelated $^{40}Ar/^{36}Ar$ and ^{36}Ar concentration values. Metamophic fluids derived from crystalline rocks are likely to have Air Saturated Water (ASW = 1.3–2.7 ppb) or lower ^{36}Ar concentrations. The $^{40}Ar/^{36}Ar$ value and

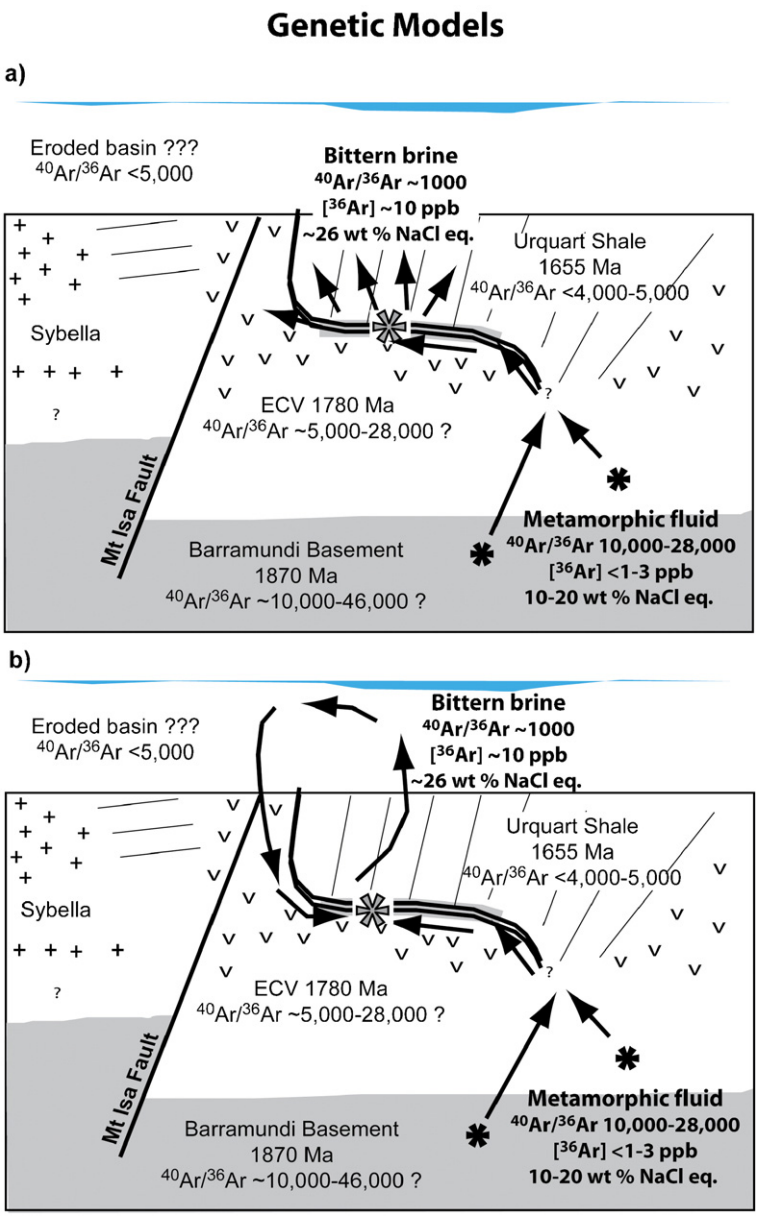

Fig. 14. Schematic diagrams indicating two mineralization models compatible with the noble gas and halogen data; (a) fluid displacement model; (b) active convection model. Mineralisation in these models occurred at ~1530 Ma, synchronous with post-peak metamorphism of the Sybella Batholith and D_3 deformation that may have reactivated Paroo 'thrust' Fault (Perkins, 1984; Swager, 1985; Connors and Page, 1995; Perkins et al., 1999).

$^{40}Ar_E$ concentration is determined by the source region mineralogy, K content and age, the $^{40}Ar/^{36}Ar$ value could be as low as 296 or even higher than the MORB value of 44,000 (Ozima and Podosek, 2002).

- Surface-derived sedimentary formation waters may acquire significantly elevated $^{40}Ar/^{36}Ar$ values, similar to those of metamorphic fluids (tens of thousands). However, in the absence of phase separation (i.e. fluid boiling), the $^{40}Ar/^{36}Ar$ value will be positively correlated with the ^{36}Ar concentration. Surface-derived fluids with high $^{40}Ar/^{36}Ar$ values will therefore have ^{36}Ar concentrations of significantly greater than Air Saturated Water (>1.3–2.7 ppb).
- The current noble gas and halogen data favour mixing between a deeply derived metamorphic fluid best preserved in main-stage quartz fluid inclusions and a

surface-derived sedimentary formation water with bittern brine origin best preserved in dolomite fluid inclusions.
- The lowest Br/Cl value of $\sim 1.5 \times 10^{-3}$ measured in dolomite fluid inclusions is similar to the modern-day seawater value. This may indicate Proterozoic seawater had a similar Br/Cl value, and it is compatible with the acquisition of salinity by sub-aerial evaporation.
- The Br/Cl value of the metamorphic fluid preserved in quartz fluid inclusions, may have been significantly fractionated by wall rock interaction at a very low water-rock ratio in an initially rock-buffered system. However, the data are compatible with the conservative behaviour of Br/Cl at the site of mineralization, where higher water-rock ratios predominated (fluid-buffered), and mixing of fluids with independent origins is inferred to have been responsible for the total Br/Cl variation.

Acknowledgements

This work was funded by the pmd*CRC (Predictive Mineral Discovery Cooperative Research Centre) H4 and H6 projects and is published with permission. Stanislav Szczepanski is thanked for technical assistance in the laboratory. MK would like to thank John Miller for providing valuable insight of the mine's structural geology. We also thank Andy Wilde for assistance in sample acquisition and his initial enthusiasm for the project. Patrick Williams and an anonymous reviewer are gratefully acknowledged for constructive reviews that improved the clarity of this manuscript, and Dave Rickard is thanked for his careful editorial handling.

Appendix A. Supplementary data

Supplementary data associated with this article can be found, in the online version, at doi:10.1016/j.chemgeo.2006.08.002.

References

Allegre, C.J., Staudacher, Th., Sarda, Ph., 1987. Rare gas systematics: formation of atmosphere, evolution and structure of the Earth's mantle. Earth and Planetary Science Letters 81, 127–150.

Andrew, A.S., Heinrich, C.A., Wilkins, R.W.T., Patterson, D.J., 1989. Sulfur isotope systematic sod copper ore formation at Mount Isa, Australia. Economic Geology 84, 1614–1626.

Bain, J.H.C., Heinrich, C.A., Henderson, G.A.M., 1992. Stratigraphy, structure and metasomatism of the Haslingden Group, east Moondara area, Mount Isa: a deformed and mineralised Proterozoic multistage rift-sag sequence. Australian Bureau of Mineral Resources Geology and Geophysics Bulletin 243, 125–136.

Bell, T.H., 1983. Thrusting and duplex formation at Mount Isa, Queensland, Australia. Nature 304, 493–497.

Bell, T.H., Perkins, W.G., Swager, C.P., 1988. Structural controls on development and localization of syntectonic copper mineralization at Mount Isa, Queensland. Economic Geology 83, 69–85.

Betts, P.G., et al., 2006. Synthesis of the Proterozoic evolution of the Mt. Isa Inlier. Australian Journal of Earth Sciences 53, 187–211.

Böhlke, J.K., Irwin, J.J., 1992a. Brine history indicated by argon, krypton, chlorine, bromine, and iodine analyses of fluid inclusions from the Mississippi Valley type lead-fluorite-barite deposits at Hansonburg, New Mexico. Earth and Planetary Science Letters 110, 51–66.

Böhlke, J.K., Irwin, J.J., 1992b. Laserprobe analyses of Cl, Br, I, and K in fluid inclusions: implications for the sources of salinity in some ancient hydrothermal fluids. Geochimica et Cosmochimica Acta 56, 203–225.

Carpenter, A.B., Trout, M.L., Pickett, E.E., 1974. Preliminary report on the origin and chemical evolution of lead-and zinc-rich oil field brines in central Mississippi. Economic Geology 69, 1191–1206.

Carr, G.R., Denton, G.J., Parr, J., Sun, S., Korsch, M.J., Bodon, S.B., 2004. Lightning does strike twice: multiple ore events in major mineralised systems in northern Australia. Predictive Mineral Discovery Under Cover. SEG, Perth.

Connors, K.A., Page, R.W., 1995. Relationships between magmatism, metamorphism and deformation in the western Mount Isa Inlier, Australia. Precambrian Research 71, 131–153.

Davis, T., 2004. Mine-scale structural controls on the Mount Isa Zn–Pb–Ag and Cu orebodies. Economic Geology 99, 543–559.

Derrick, G.M., 1976. Mary Kathleen Queensland geological map: Geoscience Australia, no. 20439, scale: 1:100,000.

Drescher, J., Kirsten, T., Schäfer, K., 1998. The rare gas inventory of the continental crust, recovered by the KTB Continental Deep Drilling Project. Earth and Planetary Science Letters 154, 247–263.

Duncan, R.J., Wilde, A.R., Bassano, K., Maas, R., 2006. Geochronological constraints on tourmaline formation in the Western Fold Belt of the Mount Isa Inlier, Australia: evidence for large-scale metamorphism at 1.57 Ga? Precambrian Research 146, 120–137.

Farquharson, R.B., Richards, J.R., 1974. U–Th–Pb Isotopic systematics related to igneous rocks and ore Pb, Mount Isa, Queensland. Mineralium Deposita 9, 339–356.

Hand, M., Rubatto, D., 2002. The scale of the thermal problem in the Mt. Isa Inlier. The 16th Australian Geological Conference. Geological Society of Australia Abstracts, p. 173.

Hannan, K.W., Golding, S.D., Herbert, H.K., Krouse, H.R., 1993. Contrasting alteration assemblages in metabasites from Mount Isa, Queensland: implications for copper ore genesis. Economic Geology 88, 1135–1175.

Hanor, J.S., 1994. Origin of saline fluids in sedimentary basins. In: Parnell, J. (Ed.), In Geofluids: Origin, migration and Evolution of Fluids in Sedimentary Basins. Geological Society Special Publication, pp. 151–174.

Heinrich, C.A., Andrew, A.S., Wilkins, R.W.T., Patterson, D.J., 1989. A fluid inclusion and stable isotope study of synmetamorphic Copper Ore Formation at Mount Isa, Australia. Economic Geology 84, 529–550.

Heinrich, C.A., Bain, J.H.C., Fardy, J.J., Waring, C.L., 1993. Br/Cl geochemistry of hydrothermal brines associated with Proterozoic metasediment-hosted copper mineralization at Mount Isa, northern Australia. Geochimica et Cosmochimica Acta 57, 2991–3000.

Heinrich, C.A., Bain, J.H.C., Mernagh, T.P., Wyborn, L.A.I., Andrew, A.S., Waring, C.L., 1995. Fluid and mass transfer during

metabasalt alteration and copper mineralization at Mount Isa, Australia. Economic Geology 90, 705–730.
Hill, R.M., 1978. Mt. Isa Queensland geological map, 1978, scale 100,000.
Holser, W.T., 1979. Trace elements and isotopes in evaporites. In: Burns, R.G. (Ed.), Marine Minerals. Reviews in Mineralogy, vol. 6. Mineralogical Society of America, Washington D.C, pp. 295–346.
Irwin, J.J., Reynolds, J.H., 1995. Multiple stages of fluid trapping in the Stripa granite indicated by laser microprobe analysis of Cl, Br, I, K, U, and nucleogenic plus radiogenic Ar, Kr and Xe in fluid inclusions. Geochimica et Cosmochimica Acta 59, 355–369.
Irwin, J.J., Roedder, E., 1995. Diverse origins of fluid inclusions at Bingham (Utah, USA), Butte (Montana, USA), St. Austell (Cornwall, UK) and Ascension Island (mid-Atlantic, UK), indicated by laser microprobe analysis of Cl, K, Br, I, Ba^{+}, Te, U, Ar, Kr, and Xe. Geochimica et Cosmochimica Acta 59 (2), 295–312.
Jackson, M.J., Scott, D.L., Rawlings, D.J., 2000. Stratigraphic framework for the Leichhardt and Calvert Siperbasins: review and correlations of the pre-1700 Ma successions between Mt. Isa and McArthur River. Australian Journal of Earth Science 47, 381–403.
Kelley, S., Turner, G., Butterfield, A.W., Shepherd, T.J., 1986. The source and significance of argon isotopes in fluid inclusions from areas of mineralization. Earth and Planetary Science Letters 79, 303–318.
Kendrick, M.A., Burgess, R., Pattrick, R.A.D., Turner, G., 2001a. Noble gas and halogen evidence on the origin of Cu-Porphyry mineralising fluids. Geochimica et Cosmochimica Acta 65, 2651–2668.
Kendrick, M.A., Burgess, R., Pattrick, R.A.D., Turner, G., 2001b. Halogen and Ar–Ar age determinations of inclusions within quartz veins from porphyry copper deposits using complementary noble gas extraction techniques. Chemical Geology 177, 351–370.
Kendrick, M.A., Burgess, R., Leach, D., Pattrick, R.A.D., 2002a. Hydrothermal fluid origins in Mississippi valley-type ore deposits: combined noble gas (He, Ar, Kr) and halogen (Cl, Br, I) analysis of fluid inclusions from the Illinois-Kentucky Fluorspar district, Viburnum Trend, and Tri-State districts, mid-continent United States. Economic Geology 97 (3), 452–479.
Kendrick, M.A., Burgess, R., Pattrick, R.A.D., Turner, G., 2002b. Hydrothermal fluid origins in a fluorite-rich Mississippi valley-type deposit: combined noble gas (He, Ar, Kr) and halogen (Cl, Br, I) analysis of fluid inclusions from the South Pennine Orefield, United Kingdom. Economic Geology 97 (3), 435–451.
Kendrick, M.A., Burgess, R., Harrison, D., Bjørlykke, A., 2005. Noble gas and halogen evidence on the origin of Scandinavian sandstone-hosted Pb–Zn deposits. Geochimica et Cosmochimica Acta 69, 109–129.
Kendrick, M.A., Miller, J.M., Phillips, D., 2006a. Part I. Decrepitation and degassing behaviour of quartz up to 1560 C: Analysis of noble gases and halogens in complex fluid inclusions assemblages. Geochimica et Cosmochimica Acta 70, 2540–2561.
Kendrick, M.A., Miller, J.M., Phillips, D., 2006b. Part II. Evaluation of 40Ar-39Ar quartz ages: Implications for fluid inclusion retentivity and determination of initial 40Ar/36Ar values in Proterozoic samples. Geochimica et Cosmochimica Acta 70, 2562–2576.
Kesler, S.E., Appold, M.S., Martini, A.M., Walter, L.M., Huston, T.J., Kyle, J.R., 1995. Na–Cl–Br systematics of mineralising brines in Mississippi Valley-type deposits. Geology 23, 641–644.
Lister, G.S., Thomas, A., Dunn, J., 1986. Tectonic processes in the Mt. Isa Inlier; the significance of transpressional strike slip faulting. Geological Society of Australia Abstracts 15, 127–128.
Lister, G.S., O'Dea, M.G., Somaia, I., 1999. A tale of two synclines: rifting, inversion and transpressional popouts at Lake Julius, northwestern Mount Isa Terrane, Queensland. Australian Journal of Earth Sciences 46, 233–250.
MacCready, T., Goleby, B.R., Goncharov, A., Drummond, B.J., Lister, G.S., 1998. A framework of overprinting orogens based on interpretation of the Mt. Isa deep seismic transect. Economic Geology 93, 1422–1434.
Mathias, B.V., Clark, G.J., 1975. Mount Isa copper and silver-lead-zinc orebodies—Isa and Hilton Mines. Australasian Institute of Mining and Metallurgy Monograph 5, 351–372.
Matthai, S.K., Heinrich, C.A., Driesner, T., 2004. Is the Mount Isa copper deposit the product of forced brine convection in the footwall of a major reverse fault? Geology 32, 357–360.
McCaffrey, M.A., Lazar, B., Holland, H.D., 1986. The evaporation path of seawater and the composition of Br^{-} and K^{+} with halite. Journal of Sedimentary Petrology 57, 928–937.
McDonald, J.A., 1970. Some effects of deformation on sulphide-rich layers in lead-zinc ore bodies, Mount Isa, Queensland. Economic Geology 65, 273–298.
McGoldrick, P.J., 1986. Volatile and precious metal geochemistry of the Mount Isa ores and their host rocks. Unpublished PhD thesis Thesis, University of Melbourne, 330 pp.
McGoldrick, P.J., Keays, R.R., 1990. Mount Isa copper and lead-zinc-silver ores: coincident or cogenesis? Economic Geology 85, 641–650.
McGoldrick, P.J., Large, R., 1998. Proterozoic sediment-hosted Zn–Pb–Ag deposits. AGSO Journal of Australian Geology and Geophysics 17, 189–196.
Neudert, M.K., 1983. A depositional model for the Mount Isa Group and implications for ore formation. Unpublished PhD thesis Thesis, Australian National University, 324 pp.
Neudert, M.K., Russel, R.E., 1981. Shallow water and hypersaline features from the middle Proterozoic Mt. Isa sequence. Nature 293, 284–286.
Neumann, N. L., Southgate, P. N., Gibson, G. M., McIntyre, A., in press. New SHRIMP geochronology for the Western Fold Belt of the Mt. Isa Inlier: developing a 1800–1650 Ma event framework. Australian Journal of Earth Sciences 53 (6).
O'Dea, M.G., Lister, G.S., MacCready, T., Betts, P.G., Oliver, N.H.S., Pound, K.S., Huang, W., Valenta, R.K., 1997. Geodynamic evolution of the Proterozoic Mount Isa terrain. In: Burg, J.P., Ford, M. (Eds.), Orogeny through Time. Special Publication. Geol. Soc. London, pp. 99–122.
Ozima, M., Podosek, F.A., 2002. Noble Gas Geochemistry. Cambridge University Press.
Page, R.W., Bell, T.H., 1986. Isotopic and structural responses of granite to successive deformation and metamorphism. Journal of Geology 94, 365–379.
Page, R.W., Williams, I.S., 1988. Age of the Barramundi Orogeny in northern Australia by means of ion microprobe and conventional U–Pb studies. Precambrian Research 40/41, 21–36.
Page, R.W., Jackson, M.J., Krassay, A.A., 2000. Constraining sequence stratigraphy in north Australian basins: SHRIMP U–Pb zircon geochronology between Mt. Isa and McArthur River. Australian Journal of Earth Sciences 47, 431–459.
Perkins, W.G., 1984. Mount Isa silica dolomite and copper orebodies: The result of a syntectonic hydrothermal alteration system. Economic Geology 79, 601–637.
Perkins, W.G., Bell, T.H., 1998. Stratiform replacement lead-zinc deposits: a comparison between Mt. Isa, Hilton, and McArthur River. Economic Geology 93, 1190–1212.

Perkins, C., Heinrich, C.A., Wyborn, L.A.I., 1999. 40Ar/39Ar Geochronology of Copper Mineralisation and Regional Alteration, Mount Isa, Australia. Economic Geology 94, 23–36.

Rubenach, M.J., 1992. Proterozoic low-pressure/high temperature metamorphism and an anticlockwise *P–T–t* path for the Hazeldene area, Mount Isa Inlier. Journal of Metamorphic Geology 10, 333–346.

Schilling, J.G., Unni, C.K., Bender, M.L., 1978. Origin of chlorine and bromine in the oceans. Nature 273, 631–636.

Shinonaga, T., Ebihara, M., Nakahara, H., Tomura, K., Heumann, K.G., 1994. Cl, Br, I in igneous standard rocks. Chemical Geology 115, 213–225.

Smith, S.P., Kennedy, B.M., 1983. The solubility of noble gases in water and in NaCl brine. Geochimica et Cosmochimica Acta 47, 503–515.

Southgate, P.N., et al., 2000. Chronostratigraphic basin framework for Palaeoproterozoic rocks (1730–1575 Ma) in northern Australia and implications for base-metal mineralization. Australian Journal of Earth Sciences 47, 461–483.

Spikings, R.A., Foster, D.A., Kohn, B.P., Lister, G.S., 2002. Post-orogenic (<1500 Ma) thermal history of the Palaeo-Mesoproterozoic, Mt. Isa province, NE Australia. Tectonophysics 349, 327–365.

Svensen, H., Banks, D.A., Austreim, H., 2001. Halogen contents of eclogite facies fluid inclusions and minerals: Caledonides, western Norway. Journal of Metamorphic Geology 19, 165–178.

Swager, C.P., 1985. Syndeformational carbonate-replacement model for the copper mineralisation at Mount Isa, Northwest Queensland: a microstructural study. Economic Geology 80, 107–125.

Turner, G., Bannon, M.P., 1992. Argon isotope geochemistry of inclusion fluids from granite-associated mineral veins in southwest and northeast England. Geochimica et Cosmochimica Acta 56, 227–243.

Viets, J.G., Hofstra, A.H., Emsbo, P., 1996. Solute composition of fluid inclusions in sphalerite from North American and European Mississippi valley-type ore deposits: ore fluids derived from evaporated seawater. Society of Economic Geologists Special Publication 4, 465–482.

Walter, L.M., Stueber, A.M., Huston, T.J., 1990. Br–Cl–Na systematics in Illinois basin fluids: constraints on fluid origin and evolution. Geology 18, 315–318.

Waring, C.L., 1990. Genesis of the Mount Isa Cu ore system. Ph.D. Thesis Thesis, Monash University, Melbourne, 409 pp.

Waring, C.L., Heinrich, C.A., Wall, V.J., 1998. Proterozoic metamorphic copper deposits. AGSO Journal of Australian Geology and Geophysics 17, 239–246.

Worden, R.H., 1996. Controls on halogen concentrations in sedimentary formation waters. Mineralogical Magazine 60, 259–274.

Yanatieva, O.K., 1946. Polythermal solubilities in the systems $CaCl_2$–$MgCl_2$–H_2O and $CaCl_2$–NaCl–H_2O. Zhurnal Prikladnoi Khimii 19, 709–722 (in Russian).

Zherebtsova, I.K., Volkova, N.N., 1966. Experimental study of behaviour of trace elements in the process of natural solar evaporation of Black Sea water and Lake Sasky-Sivash brine. Geochemistry International 3, 656–670.